STUDY ON CATALYTIC STEAM CRACKING OF ETHANE OVER NICKEL PHOSPHIDE CATALYSTS

PANISA HONGKLAI

A THESIS SUBMITTED IN PARTIAL FULFILLMENT OF

THE REQUIREMENT FOR THE DEGREE OF

MASTER OF SCIENCE IN APPLIED CHEMISTRY

DEPARTMENT OF CHEMISTRY SCHOOL OF SCIENCE

KING MONGKUT'S INSTITUTE OF TECHNOLOGY LADKRABANG

2022

KMITL-2022-SC-M-012-088

Thesis Title	Study on catalytic steam cracking of ethane over nickel phosphide catalysts
Student Name	Miss Panisa Hongklai
Student ID	60605027
Degree	Master of Science (Applied chemistry)
Department	Chemistry
Year	2022
Thesis Advisor	Asst. Prof. Dr. Kittisak Choojun
Thesis Co-Advisor	Prof. Dr. Tawan Sooknoi

Abstract

The formation of Ni_2P over a support (TiO_2 and SiO_2) using different P/Ni molar ratio (0.5 and 2.0) for the preparation was studied. For Ni_xP_y/TiO_2-0.5P prepared by P/Ni molar ratio of 0.5, the mixture of Ni_2P and $Ni_{12}P_5$ species was observed by XRD and ^{31}P MAS-NMR. In sharp contrast, under excess phosphate precursor (P/Ni molar ratio of 2.0) for Ni_2P/TiO_2-2.0P, pure Ni_2P was obtained. According to the *in-situ* TR-XANES, Ni_2P/TiO_2-0.5P showed the reduction at 500˚C which is quite similar to reduction of NiO in Ni/TiO_2. However, Ni_2P/TiO_2-2.0P showed a much higher reduction temperature at 650˚C, resulting from the reduction of $Ni_2P_4O_{12}$ that could be mainly formed under excess phosphorous precursor. For both samples, once Ni_2P was evidenced only after the metallic Ni formed. Ni_2P was successfully prepared over TiO_2(Anatase) and SiO_2 using P/Ni molar ratio of 2.0, regardless to the different surface areas of these supports. Ni_2P/TiO_2-2.0P provided >99% ethylene selectivity from ethane steam cracking at 650˚C with ethane conversion rate of 65.2 $mmol_{ethane} \cdot g_{Ni}^{-1} \cdot h^{-1}$. While none of ethylene was observed over Ni/TiO_2 catalyst. A lower in ethane conversion rate was observed over Ni_2P/TiO_2-2.0P due to the lower Ni_2P content. Due to the lower surface area of Ni_2P/TiO_2(anatase)-2.0P, a lower activity was obtained. The catalysts without strong metal support interaction (Ni_2P/SiO_2-2.0P and Ni_2P/TiO_2(Phy) resulted in the lower

activity as compared to Ni_2P/TiO_2-2.0P. The changes in nickel species from Ni_2P to Ni^0 was observed after 11 h of use and confirmed by the *in-situ* TR-XANES.

Keywords: Catalytic steam cracking, Nickel phosphide, Ni_2P, $Ni_{12}P_5$

Acknowledgement

The authors take this opportunity to Acknowledgement advisors Asst. Prof. Dr. Kittisak Choojun and Prof. Dr. Tawan Sooknoi, for the continually suggestion, graceful knowledge and useful discussion throughout this research. In addition, we would like to sincere appreciate chairperson and committee member, Assoc. Prof. Dr. Panpailin Seeharaj and Prof. Dr. Joongjai Panpranot, respectively, for the opinions and the guidance with a graceful.

We appreciate the supports from the Department of Chemistry, Faculty of Science, King Mongkut's Institute of Technology Ladkrabang.

We would like to distribute a kindness thank to Catalytic Center Research Unit members for their contribution of the ideas and facilities and most importantly their support

We would like to extend our sincere appreciation to all teachers and friends for their constant guidance advice, valuable supports and encouragement.

Finally, we deeply appreciate and thank our family for their love and kindness. The project would not be possible without them.

Miss Panisa Hongklai

Table of Contents

Table of Contents (Continued)

List of Tables

List of Figures

List of Schemes

CHAPTER 1
INTRODUCTION

1.1 Motivation

Ethylene is an important chemical feedstock for many chemical productions, such as polyethylene, polyvinyl chloride, polyethylene terephthalate, ethylene glycol, and styrene [1]. In 2017, the production of ethylene was 180 million metric tons (MMT) with a global demand of 160 MMT of ethylene [2]. The global ethylene demand growth remains strong and the expectation of demand growth is in the range of 6.5 million metric tons per year [3]. For century, petroleum is the major source to produce ethylene, mainly steam cracking process. To meet the increasing demand of ethylene while petroleum source is limited, the alternative production of ethylene remains challenges.

Rather than relying on the petroleum, production of ethylene directly from ethane has gained more attention due to two main reasons. Firstly, ethane is one of the main compositions in natural gas. Secondly, in recent decades, the advancement of hydraulic fracturing and horizontal drilling has resulted in the boom of the U.S. shale gas production. This shale gas is mainly composed of methane and ethane [4]. The proposing of shale gas would serve at least another century. Therefore, ethane could replace the obsolescent fossil-fuel-based feedstocks to produce ethylene.

Generally, ethane could convert to ethylene via two major pathways which are catalytic dehydrogenation and steam cracking process. The first reaction requires catalysts mainly involves Pt-based catalysts. Odd. *et al*. (1996) [5] studied dehydrogenation of the light hydrocarbon as propane over supported Pt and Pt–Sn catalysts. The result showed high selectivity of propylene, but catalyst deactivation can be observed with low conversion [6]. Cracking of ethane, another process to produce ethylene, is generally required high temperature resulting in the higher conversion compared with typically dehydrogenation. Jukić. *et al*. (2016) studied ethane cracking at 850 ˚C showed 100% conversion with 70% ethylene selectivity [7]. To increase the selectivity of ethylene from cracking, catalysts in the class of metal

had been introduced to this process [6, 8-14]. Chin. *et al*. (2006) [15] reported that the catalytic cracking of ethane over Ni/SiO_2 catalyst at 500 ˚C provided 98% ethane conversion with 88% selectivity. However, they showed very fast deactivation due to the coke formation. To reduce the formation of coke, the steam used as an inexpensive diluent of feed during the catalytic cracking. The test in cracking/steam regeneration at 650 ˚C of 15 wt.% Ni/SiO_2 catalyst showed that the catalyst can be fully regenerated with steam in successive cycles without any significant loss of catalytic activity otherwise, the catalysts showed deactivation with time [16]. Catalytic steam cracking can inhibit the coke formation via competitive adsorption with a coke precursor on the surface of catalyst and decrease operating temperature by feed diluent as mention in Sarris. *et al.* (2017) [17]. However, to operate under steam condition, these noble metals are not tolerated by water in feed.

Recently, transition metal phosphide catalysts have been reported to operate and durable under steam even in the extreme condition [18]. Furthermore, they show the good catalytic performances for hydrotreating process, such as hydrodenitrogenation [19] and hydrodeoxygenation [20, 21]. Among the transition metal phosphide catalysts, Nickel phosphide is known to show the best activity in hydrotreating process especially for hydrodesulfurization [22-25]. Furthermore, Kim. *et al*. (2014) [26], showed that Ni_2P/zeolite catalysts can be used for naphthalene hydrocracking to BTX. The Ni_2P/Beta exhibited best activity with a naphthalene conversion of 99%, and a BTX yield of 94.4%.

Nickel phosphides have many species, e.g. Ni_2P, Ni_3P_5, Ni_5P_{12}, $Ni_{12}P_5$ [27]. However, the most active species of nickel phosphides are Ni_2P and $Ni_{12}P_5$ which can be synthesized by using different P/Ni ratios of $Ni(NO_3)_2.6H_2O$ and $(NH_4)_2HPO_4$ precursors [6]. Not only the nickel phosphide species have an effect towards the activity, their supported metal oxide also has an influence [28]. Li. *et al*. (2010) [29] reported that TiO_2 and CeO_2 are effective promoters to enhance the hydrogenation activity of Ni_2P. Wang. *et al*. (2009) [30] also showed that Ni_2P/TiO_2 - Al_2O_3 was more active than Ni_2P/Al_2O_3 for hydrodesulfurization of 3-methylthiophene.

With these reasons, we are interested in the used of nickel phosphide over support as a catalyst for steam cracking of ethane to increase ethylene production.

Moreover, the study on effect of difference P/Ni ratio, reduction time for preparation and several common metal oxides supports such as, silica (SiO_2) and titania (TiO_2) will be investigated. The catalytic performance of ethane steam cracking over the prepared catalysts will be studied including, reaction temperature, feed/steam ratio, thermal and chemical stability.

1.2 Objective

1.2.1 To synthesize the nickel phosphide catalysts.

1.2.2 To understand the physical and chemical properties of each nickel phosphide catalyst.

1.2.3 To study the catalytic performance of nickel phosphide catalysts for ethane steam cracking.

1.3 Scopes of study

1.3.1 Catalyst preparation by incipient wetness impregnation method using nickel phosphide 10 wt.% loading on support as SiO_2 and TiO_2 (P25).

1.3.2 Studied phase of nickel phosphide preparation by difference P/Ni (x) ratio (where x is P/Ni = 0.5 and 2).

1.3.3 Studied phase of nickel phosphide preparation by difference reduction time (0.5, 1, 2 h) at reduction temperature 650 °C.

1.3.4 Characterization of nickel phosphide

1.3.4.1 Physical Characterization

X-ray Diffraction (XRD), ^{31}P Magic angle spinning nuclear magnetic resonance (^{31}P MAS-NMR), X-ray fluorescence (XRF), Brunauer-Emmett-Teller (BET) Surface area analysis

1.3.4.2 Chemical Characterization

in-situ Time-Resolved X-ray Near-Edge Absorption Spectroscopy (*in-situ* TR-XANES)

1.3.5 Study the catalytic activity of the prepared catalysts by the ethane conversion rate of ethane steam cracking at 650 °C. The active species of Ni, interaction and contact time will be study.

1.4 Expected result

It is expected that this study could provide a better selectivity of ethylene and high stability over supported nickel phosphide catalysts for ethane steam cracking. Moreover, the mechanistic understanding of ethane steam cracking reaction over nickel phosphide (Ni_xP_y) catalysts could design the suitable catalysts for steam cracking process.

CHAPTER 2
THEORY AND LITERATURE REVIEWS

2.1 Ethylene

Ethylene or ethene (IUPAC name) is a chemical compound with the formula C_2H_4. Each molecule contains one double bond between the two carbon atoms, and for this reason it is classified as an alkene, olefin, or unsaturated hydrocarbon. An ordinary temperature and pressure, it is a colorless gas. The H – C – H angle of ethylene is 117°. The molecule is also relatively rigid. The rotation of C = C bond requires energy because it needs to break **π**-bond; while, retaining the **σ**-bond between the carbon atoms [31].

Ethylene is widely used as a starting chemical in the polymer manufacture such as polyethylene (PE), polyethylene terephthalate (PET), polyvinylchloride (PVC) and polystyrene (PS), as well as fibers and other organic chemicals. These products are used in a wide variety of applications, such as the packaging, transportation, electrical, electronic, textile, construction industries, consumer chemicals, coatings and adhesives [1]. The largest outlet, accounting for 60% of ethylene demand globally, is polyethylene. Low density polyethylene (LDPE) and linear low density polyethylene (LLDPE) mainly go into film applications, such as food and non-food packaging, shrink and stretch film [32]. High density polyethylene (HDPE) is used primarily in blow molding and injection molding applications, such as containers, drums, household goods, caps and pallets [33]. HDPE can also be extruded into pipes for water, gas and irrigation, and film for refuse sacks, carrier bags and industrial lining [33].

Another use of ethylene to convert is ethylene oxide (EO) which is a primarily precursor for ethylene glycol. Most monoethylene glycol (MEG) is used to make polyester fibers for textile applications, PET resins for bottles, and polyester film. MEG is also used in antifreeze applications. Other EO derivatives include ethyoxylates (use in shampoo, kitchen cleaners, etc), glycol ethers (use as solvents, fuels, etc) and ethanolamines (surfactants, personal care products, etc) [34].

Ethylene dichloride (EDC) is another product deriving from the chlorination of ethylene. It can then be cracked to make vinyl chloride monomer (VCM). Nearly all

VCM is used to make polyvinyl chloride which has its main applications in the construction industry.

Ethylene can react with benzene to make ethylbenzene which is further processed into styrene. The main outlets for styrene are polymers and synthetic rubbers, such as polystyrene, acrylonitrile-butadiene-styrene (ABS) and styrene butadiene rubber (SBR). Other ethylene derivatives include alpha olefins which are used in LLDPE production, detergent alcohols and plasticizer alcohols; vinyl acetate monomer (VAM) which is used in adhesives, paints, paper coatings and barrier resins; and industrial ethanol which is used as a solvent or in the manufacture of chemical intermediates for ethyl acetate and ethyl acrylate [35].

Therefore, ethylene is one of the largest-volume petrochemicals. With a diverse range of end-uses, the demand is sensitive to both economic and energy cycles. According to US-based SRI Consulting, global production and consumption of ethylene in 2009 were both approximately 112m tones [2]. Global capacity utilization was 85.3% in 2009, down from 87% in 2008. Ethylene consumption is estimated to have increased by 1.3% in 2009; it is forecast to grow an average 4.1%/year up to 2014, slowing to 3.4%/year from 2014 to 2019.

Ethylene is mainly supplied from petrochemical industry which rely on cracking of heavy feedstocks, such as Naphtha and gas oils. Though, the concern of the depletion of petroleum drives the research to find an alternative source. Ethane dehydrogenation forming ethylene is one of promising strategy due to the large supply of ethane from natural gas and shale gas.

2.2 Ethane

Ethane is a chemical compound with the chemical formula C_2H_6. It is an aliphatic hydrocarbon classified as an alkane. At standard temperature and pressure, ethane is a colorless, odorless, flammable gas. Ethane can be industrially isolated from natural gas and petroleum refining [36]. The industrial importance of ethane is based upon the ease of a transformation to ethylene (C_2H_4) and hydrogen by a pyrolysis or cracking once it passes through a hot tube at a temperature above 1,000 ºC. Like propane and to a lesser extent butane, ethane is a major raw material for the huge ethylene petrochemical industry. Another ethane process is under investigation as a

feedstock for other commodity chemicals, such as oxidative chlorination of ethane to produce vinyl chloride.

Ethane production

Ethane is the second-largest component of natural gas (NG) in fossil fuel after methane and the exact composition of natural gas is different depending on the location as shown in **Table 2.1**.

Table 2.1 The natural gas supplied to Union Gas comes from western Canada, the United States and Ontario producers [37].

Compound	Symbol	Percent in natural gas
Methane	CH_4	60 – 90
Ethane	C_2H_6	0 – 20
Propane	C_3H_8	0 – 20
Butane	C_4H_{10}	0 – 20
Carbon dioxide	CO_2	0 – 8
Oxygen	O_2	0 – 0.2
Nitrogen	N_2	0 – 5
Hydrogen sulphide	H_2S	0 – 5
Rare gases	Ar, He	0 – 2

Alternatively, shale gas has been recognized as one of the most source to gain ethane for a century in the United States. Shale gas is natural gas trapped within tiny pore spaces in shale formations as shown in **Table 2.2** [38]. Shale gas, also known as parent rock gas or schist gas, is the same gas as we usually use for heating. However, it is trapped in rocks and schist. This means that different methods must be used to extract it out. The most well-known of method is hydraulic fracturing [39].

Table 2.2 The shale gas composition at Canada [38].

Compound	Symbol	Percent in shale gas
Methane	CH_4	74.22
Ethane	C_2H_6	15.62
Propane	C_3H_8	5.46
Butane	C_4H_{10}	1.40
Pentanes	C_5H_{12}	1.00
Hexanes	C_6H_{14}	1.00
Inerts/other	He, CO_2, O_2, etc.	1.30

2.3 Dehydrogenation

Dehydrogenation is a chemical reaction that involves the removal of hydrogen from an organic molecule as showed in **scheme 2.1**. It is the reverse of hydrogenation. Dehydrogenation is an important reaction because it converts alkanes, which are relatively inert and thus low-valued, to more reactive and value olefins (including alkenes). These alkenes are precursors to produce aldehydes, alcohols, polymers, and aromatics. Dehydrogenation are used extensively in the petrochemical industry to produce aromatics and styrene. Such processes are highly endothermic and require a temperature of 500 °C and above.

$$C_nH_{2n+2} \xrightarrow{\Delta} C_nH_{2n} + H_2 \quad \text{; cracking of C – H}$$

Scheme 2.1 Typical dehydrogenation reaction

In general, the dehydrogenation reaction can be classified into two strategies that are the direct dehydrogenation and oxidative dehydrogenation. The oxidative dehydrogenation is an exothermic reaction that requires lower reaction temperature than that of the direct dehydrogenation, which is an endothermic reaction. However, the oxidative dehydrogenation requires an oxidant, such as oxygen and halogen. Due to the oxidant use, it may cause the processes over oxidation reaction forming an unpleasant byproduct, such as carbon dioxide and halogenated organic molecule.

Considering the direct ethane dehydrogenation (EDH), ethylene and hydrogen would be the product from this reaction. This reaction is normally catalyzed by several types of catalysts. Ga supported on zeolite [40], Pd-In supported on silica [41], Pd supported on alumina [43] can successfully facilitate the dehydrogenation of ethane. The advantage of this process is the high ethylene selectivity; however, the catalyst deactivation and low conversion are generally observed [40-42].

2.4 Cracking process

Cracking process is the pathway to break down heavy hydrocarbon molecules into lighter molecules by means of heat, and sometimes catalysts. Cracking is the most important process for the commercial production of gasoline and diesel fuel from petroleum refining. Furthermore, cracking of petroleum yields heavy oils, a solid carbonaceous product known as coke, and light gases, such as methane, ethane, ethylene, propane, propylene, and butylene. These gases can be used in the refinery's fuel system. More importantly, they are raw materials for synthetic rubber, plastic and agricultural chemicals [43].

In cracking process, there are two major categories. One is the thermal cracking governing by heat as a main factor. The other is the use catalyst to enhance the conversion and selectivity [43].

2.4.1 Thermal cracking

Thermal cracking is non-catalyzed process of thermal decomposition of hydrocarbons. It is performed at very high temperatures, 750 - 900 °C, under approximately normal pressure. Cracking reactions involve the breaking of one or more covalent carbon-carbon bonds in the hydrocarbon molecules via a free radical mechanism. Consequently, a smaller molecule is formed. At the same time, C – H bond breaking can compete with C – C bond resulting the loss of hydrogen as shown in **Scheme 2.2**.

$$C_nH_{2n+2} \xrightarrow{\Delta} C_mH_{2m+2} + C_qH_{2q} \quad \text{; cracking of C – C bond}$$

$$C_nH_{2n+2} \xrightarrow{\Delta} C_nH_{2n} + H_2 \quad \text{; cracking of C – H bond}$$

Scheme 2.2 Cracking of hydrocarbon

Side reactions of thermal cracking involve isomerization, cyclization, polymerization and series of reactions of cyclodehydrogenation which are led to formation of coke (polyaromatic hydrocarbon). Such thermal cracking plant suffers coke deposition problems that restrict performance. The cracking operation involves heating heavy hydrocarbon in radiantly heated coils of high alloy steel tubing to temperatures of typically 850 °C. During cracking, coke deposition occurs in the coils and associated downstream exchangers. The coke, which forms to depths of several mm, reduces heat transfer and normally limits run length of reaction that effects to decrease activity. The cracking furnace must then be taken off-stream for decoking, usually by steam-air oxidation, with consequential loss of production [7].

2.4.2 Steam cracking

The water is added to a feed for thermal cracking called "Steam cracking." Steam cracking is the principal industrial method for producing the lighter olefins via homolytic; free radical, including ethylene and propylene. Steam cracker units are facilities in which a feedstock, such as naphtha, liquefied petroleum gas (LPG), ethane, propane or butane is thermally cracked through the use of steam in a bank of pyrolysis furnaces to produce lighter hydrocarbons. The products obtained depend on the composition of the feed, the hydrocarbon-to-steam ratio, and on the cracking temperature and furnace residence time.

Cracking at higher temperature (also referred to as severity) favors the production of ethylene and benzene, whereas lower severity produces higher amounts of propene, C4-hydrocarbons and liquid products. The process also results in the slow deposition of coke, a form of carbon, on the reactor walls. Then co-feed with steam can help to abate the coke deposit on the reactor surface [44].

2.4.3 Catalytic cracking

The catalytic cracking process involves the presence of either an acid catalyst (usually a solid acid, such as silica-alumina and zeolites) or metal-supported catalyst. This process requires lower temperature for operating than thermal and steam cracking. The catalyst promotes a heterolytic (asymmetric) breakage of bonds yielding pairs of ions in opposite charges, usually a carbocation and the very unstable hydride anion [45]. Even though catalytic cracking is providing a high activity and selectivity, it suffers from the deactivation of catalyst because of coke deposition on the surface of

a catalyst [45]. Coke formation in the catalytic cracking process causes the loss of a product and a source of heat through its combustion. This coke formation over catalyst's surface in catalytic cracking occurs mainly via the reactions of aromatic hydrocarbons formed as intermediates or products in the process [46].

2.4.4 Catalytic steam cracking

The catalytic steam cracking is a process which is a co-worker between a catalyst, to improve activity, selectivity and therefore reduced reaction temperature to around 400–430 °C and steam to decrease coke deposit on the surface of catalyst and reactor. Most of catalysts cannot be durable in extremely steam condition. This is the new pathway to improve cracking process that many researchers are interesting in the present [47].

2.5 Catalysts

2.5.1 Nickel phosphide

Transition metal phosphides have recently been reported as a new class of high-activity catalysts. These materials contain phosphorus and transition metals. They are considerate as a hardness and strength ceramic. Their electronic properties like conductivity is of similar to metallic compounds [48].

Among the transition metal phosphide catalysts, nickel phosphide (Ni_xP_y) shows the best catalytic activity in steady state system for a longer time on steam in hydrocracking process [49]. The most active species of nickel phosphides are Ni_2P and $Ni_{12}P_5$ which can be synthesized by using difference Ni/P ratio of precursors and the reduction time. The easily method to prepare nickel phosphide is co-impregnation between nickel nitrate (source of Ni) and ammonium phosphate (source of P) into supported and reduced it to form Ni_xP_y phases [49].

The crystal structure of Ni_2P and $Ni_{12}P_5$ is shown in **Figure 2.1**. The crystal structure of Ni_2P is hexagonal unit cell containing two types of Ni atoms. The Ni1 atoms are located inside of the distorted NiP_4 tetrahedral formed by four nearest phosphorus species; whereas, the Ni2 atoms are surrounded by five P neighbors 1P1 and 4P2 species forming a pyramidal environment around the central atom. For $Ni_{12}P_5$, there are two types of Ni and P sites in the tetragonal structure. The Ni1 atoms are

surrounded by the four nearest phosphorus atoms and 11 atoms forming coordination polyhedra around the Ni2 site-two nearest P atoms [49].

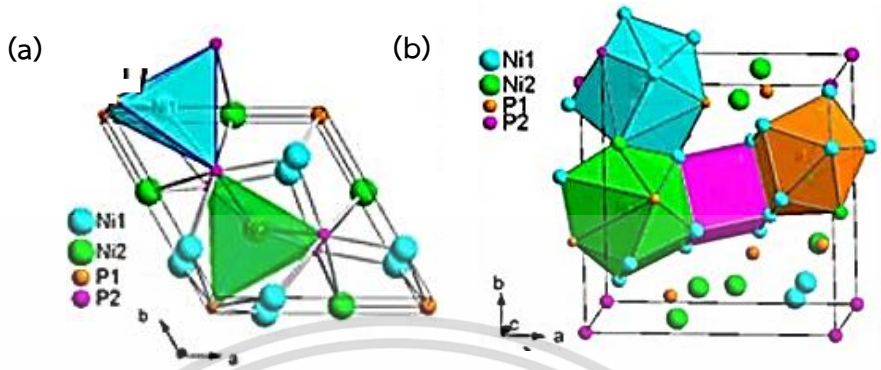

Figure 2.1 Crystal structure of (a) Ni_2P and (b) $Ni_{12}P_5$

2.5.2 Support

2.5.2.1 Silicon dioxide

Silicon dioxide, also known as silica is an oxide of silicon with the chemical formula SiO_2. The most commonly found in nature is in quartz and in various living organisms. In many parts of the world, silica is the major constituent of sand. Silica is one of the most complex and most abundant families of materials, existing as a compound of several minerals and as a synthetic product. Notable examples include fused quartz, fumed silica, silica gel, and aerogels [50]. SiO_2 has a three-dimensional network of tetrahedra cells, with four oxygen atoms surrounding each silicon ion. The tetrahedral form is the basic unit SiO_2 crystalline structure. Furthermore, amorphous SiO_2 structure is the absence of any crystalline form of SiO_2 [50]. The silica surface is nearly inert. Though, there are the –OH terminal groups (called silanol groups) weakly acidic comparable to alcohols. The terminal silanol can be removed by dehydroxylation. Two types of silanol groups are usually distinguished, isolated groups and neighboring (vicinal) groups that may be hydrogen bonded to each other. Furthermore, when calcined the fully hydrated sample at temperatures < 200 °C, They could contain germinal groups, $=Si(OH)_2$. The complete removal of silanol groups requires calcination at temperature higher than 700 °C and results in significant changes in surface morphology. The aprotic sites present after dehydroxylation at 600-800 °C have been suggested to be primarily highly strained Si-O-Si linkages.

2.5.2.2 Titanium dioxide

TiO_2 powder (Degussa, P-25), which is a standard material in the field of photocatalytic reactions, contains anatase and rutile phases in a ratio of about 3:1. Transmission electron microscopy showed that the anatase and rutile particles are separately form their agglomerates. The average sizes of the anatase and rutile elementary particles are 85 and 25 nm, respectively [51-53]. This material have an oxygen vacancy site, that is generally described as the active sites. Such a vacancy on the surface can be generated via UV-irradiation, annealing, calcination, particle bombardment, or the reaction of the solid with reducing gas such as hydrogen [51]. The presence of an oxygen vacancy site might also induce the reduction of the metal atoms into a lower oxidation number, i.e., a Ti^{3+} defect in TiO_2. The catalytic activity of TiO_2 is dependent on the nature and the composition of the surface defect sites [52]. Consider the formation of an oxygen vacancy and Ti^{3+} defects by the treatment of TiO_2 with H_2 gas as an example [53]. Initially, hydrogen gas was adsorbed on the surface of TiO_2 at high temperature. An electron from hydrogen atom was then transferred to the lattice oxygen of TiO_2. Secondly, the lattice oxygen reacts with hydrogen gas, forming water molecules. Water molecules desorbs form the surface, resulting in an oxygen vacancy site. Finally, the electron remaining there at the oxygen vacancy site could transfer to an adjacent Ti^{4+}, thereby forming the Ti^{3+} defect [37].

2.6 Literature reviews

Ethylene directly produced from ethane has gained more attention because the economically feasible of shale gas which has been developed in United State. Shale gas production provides a tremendous amount of ethane which is an alternative replacement of the non-renewable fossil-fuel-based feedstocks [7].

In general, ethylene production from ethane can be produced via catalytic dehydrogenation and steam cracking process. For the dehydrogenation reaction, current research mainly focusses on Pt-based and modified Pt-based catalysts because it activates C – H bonds more favorable than C – C bond [56-62]. Baria. *et al*. (1996) [5] reported dehydrogenation of the light hydrocarbon as propane over supported Pt and Pt–Sn catalysts and the light hydrocarbon model as propane at 519 °C. They showed that the initial selectivity of propylene is approximately 85% and 95% for Pt/γ-Al_2O_3

and PtSn/γ-Al_2O_3, respectively. The catalyst deactivation can observe in this research start with 1.2 mol% of propane and dropped to 0.9 mol% of propane (this mol% of propane result by TOF of PtSn/γ-Al_2O_3) and for Pt/γ-Al_2O_3 start from 0.8 and decreased to 0.1 mol% of propane. The advantage of this process is the high ethylene selectivity. However, the catalyst deactivation (from coke deposition) and low conversion are generally observed.

Another process is ethane steam cracking process, it has been practiced for many years in order to produce the basic feedstocks of the petrochemical industry. Steam cracking process is generally required high temperature resulting in the higher conversion compared with typically dehydrogenation. Goethema. *et al*. (2013) [54] studied ethane cracking for optimal ethylene yield with a linear-concave optimal temperature profile along the reaction coordinate with a maximum temperature between 827 and 1127 ˚C. It appears that conversion of ethane is increased from 75% to 89% with temperature 827 ˚C to 1127 ˚C, respectively. At temperature 1027 ˚C is optimal for getting a highest ethylene yield (about 67 wt%) in the steam cracking of ethane.

To increase the selectivity of ethylene cracking, the catalyst has been introduced [33-40]. Chin. *et al*. (2006) [15] reported that the catalytic cracking of ethane over Ni/SiO_2 catalyst at temperature 500 ˚C provides 95% ethane conversion with 88% selectivity. When the conversion increases to 100% at 600-650 ˚C, the ethylene selectivity dropped by 27%. Furthermore, they showed very fast deactivation due to the coke formation. To reduce the formation of coke, the steam used as an inexpensive diluent of feed during the catalytic cracking. Steam can facilitate to inhibit coke formation via competitive adsorption with coke precursor on the surface and decrease operating temperature by feed diluent as mentioned in Sarris. *et al*. (2015) [17]. Dutta. *et al*. (1999) [55], Studied effect of steam on coking chemistry of Athabasca bitumen at 450 ˚C. The result showed that coke yield with and without water exceeds 20% after 60 minutes. This is because a closed reactor is used for this study. The volatiles produced in the cracking of bitumen can further crack to produce gas or recombine to produce coke. In the presence of steam, coke yield is reduced from 24% to 21%. However, to operate under steam condition, these noble metals are not tolerated by water in feed.

Nowadays, transition metal phosphide catalysts have been reported to operate and durable under steam even in the extreme condition [18]. Furthermore, transition metal phosphides have been tested in various hydrotreating process, such as hydrogenation [56], hydrodesulfurization [57-60], hydrodenitrogenation [19] and hydrodeoxygenation [20, 21]. Among the transition metal phosphide catalysts, Nickel phosphide catalyst is known to show the best activity in hydrotreating process [22-25] for especially for hydrodesulfurization. For the example, Shu. *et al*. (2005) [48] studied the hydrodesulfurization (HDS) of 4,6-dimethyldibenzothiophene (4,6-DMDBT) on a series of supported nickel phosphide catalysts of low (Ni_2P/SiO_2-L, 96 $m^2\ g^{-1}$), medium (Ni_2P/SiO_2-M, 133 $m^2\ g^{-1}$), and high (Ni_2P/SiO_2-H, 208 $m^2\ g^{-1}$) specific surface areas. The best catalyst, Ni_2P/SiO_2-H, gave a steady-state conversion of 99% at temperature 340 °C, even after 100 h of reaction. The best selectivity for direct desulfurization is Ni_2P/SiO_2-L which give 44% of 3,3'-Dimethylbiphenyl (DMBP). There is a literature reporting performance of Ni_2P on the catalytic hydrocracking. Kim. *et al*. (2014) [26], studied Novel Ni_2P/zeolite catalysts for naphthalene hydrocracking to BTX. The catalytic activity was tested at 400 °C and 3.0 MPa in a three-phase fixed bed reactor for hydrocracking of naphthalene. The Ni_2P/Beta exhibited best activity with a naphthalene conversion of 99%, and a BTX yield of 94.4%.

Most research using nickel phosphide with the support to improve surface area of catalysts because bulk nickel phosphide has a small surface area which give low activity [27, 29, 30]. Li. *et al*. (2010) [29] indicates that bulk Ni_2P possesses low hydrogenation activity but is tunable by simply controlling the content of the additives (TiO_2 or CeO_2). They showed that TiO_2 and CeO_2 are effective promoters to enhance the hydrogenation activity of Ni_2P. Nickel phosphide on different supports shows different activity. Wang. *et al*. (2009) [30] studied the catalytic performance for hydrodesulfurization of 3-methyl thiophene on Ni_2P/TiO_2-Al_2O_3 compared with Ni_2P/Al_2O_3. The result showed the conversion of 3-MT on the Ni_2P/TiO_2-Al2O_3 catalyst is close to 100%, while the conversion of 3-MT on the Ni_2P/Al_2O_3 catalyst is nearly 85% under the temperature 330 °C, pressure 2.0 MPa and volume ratio of hydrogen/oil = 400.

Nickel phosphides have many species, e.g., Ni_2P, Ni_3P_5, Ni_5P_{12}, and $Ni_{12}P_5$ [27]. However, the most active species of nickel phosphides are Ni_2P and $Ni_{12}P_5$ which can

be synthesized by using different Ni/P ratio [6]. Oyama. *et al*. (2002) [25] used $Ni(NO_3)_2.6H_2O$ and $(NH_4)_2HPO_4$ as a precursor with Ni/P ratio = 2/1, 1/1, 1/2, 1/3 to prepared supported nickel phosphide catalysts by co-impregnation. Then the sample was dried at 120 ˚C for 3 h and calcined at 500 ˚C for 6 h after that temperature-programmed reduction (TPR) was utilized to convert the phosphate into phosphide with H_2 flow rate 110 mL/min at 650 ˚C for 2 h. At the end of the temperature program, the sample was cooled in helium to room temperature and was passivated in a 0.5% O_2/He flow for 2 h. The characterization showed the sample with the lowest P content (Ni/P ratio = 2/1) contains two phases (Ni_2P and $Ni_{12}P_5$) in the product, while the samples with the higher P contents (Ni/P ratio =1/1, 1/2, 1/3) had just one phase, Ni_2P. Guan. *et al*. (2013) [61] used $Ni(NO_3)_2.6H_2O$ and $(NH_4)_2HPO_4$ as a precursor with Ni/P ratio = 2/1 co-impregnation on support with dried sample at 120 ˚C for 3 h and calcined at 500 ˚C for 2 h, follow by varies reduction time from 10-60 min at 600 ˚C under H_2 flow 60 mL/min. Finally, the product was cooled to ambient temperature under flowing H_2 and was passivated for 1 h under flowing 1% O_2/N_2. The results clearly show that the product changes from $Ni_{12}P_5$ to Ni_2P with time and that Ni_2P can be synthesized in 60 min. The key factors in the synthesis of Ni_2P and $Ni_{12}P_5$ species depend on the reduction time and mole ratio of Ni/P in the synthesis.

Considering the possibility that nickel phosphide over support could convert ethane by catalytic steam cracking to increase ethylene production under the extreme condition. In this project will study the effect of difference P/Ni ratio, time to reduced catalyst and several common metal oxides supports such as, silica (SiO_2) and titania (TiO_2) will be used to synthesize supported Ni_2P and the catalytic performance will be investigated and compared. In addition, several factors affected to ethane steam cracking such as, reaction temperature, feed/steam ratio, thermal and chemical stability of catalysts will also be investigated.

CHAPTER 3

EXPERIMENTAL DETAILS

3.1 Reagents

	Chemicals	Grade of Purity	Manufactures
1.	TiO_2 (P-25)	-	-
2.	Silica Gel	High purity	Italmar
3.	$Ni(NO_3)_2.6H_2O$	Analytical	CARLO ERBA
4.	$(NH_4)_2HPO_4$	AR	QRëC™
5.	Nitric acid	69.50%	CARLO ERBA
6.	Ethane gas	99.50%	Linde
7.	Air (zero gas)	High purity (99.99%)	PRAXAIR
8.	Nitrogen gas	High purity (99.99%)	PRAXAIR
9.	Hydrogen gas	High purity (99.99%)	PRAXAIR
10.	Helium gas	High purity (99.99%)	PRAXAIR
11.	Gas mixture (C1-C6), 5190-0519	-	AGILENT TECHNOLOGIES
12.	*n*-Hexane	AR	QRëC™
13.	Benzene	AR	BDH
14.	Cyclohexane	AR	CARLO ERBA
15.	Heptane	AR	CARLO ERBA
16.	Toluene	99.5%	IRPC
17.	Octane	AR	CARLO ERBA
18.	Ethyl-benzene	AR	Merck
19.	Xylene	AR	CARLO ERBA
20.	Dodecane	99%	ARCOS
21.	Distilled water	-	-
22.	NaClO	-	Kao
23.	KOH	AR	CARLO ERBA

3.2 Apparatus

1. Laboratory glassware
2. Laboratory plasticware
3. Oven
4. Universal pH paper
5. Muffle Furnace
6. Alumina crucible
7. Jade mortar and pestle
8. Vacuum filter set
9. Tube furnace with a programmable temperature controller
10. Quartz tube
11. Quartz wool
12. Quartz beads
13. Quartz rod
14. Syringe (50 mL)
15. Syringe pump (KD Scientific)
16. Mass flow controller
17. Catalytic testing rig
18. Gas Chromatograph (Varian chrompack, CP-3800)
19. Diffusion Reflection Ultraviolet, DRS
20. X-ray Diffractometer, XRD (Shimadzu model XRD-6100, Scientific Instrument, KMITL)
21. Thermogravimetric analyzer (Perkin-Elmer, Scientific Instrument Service Centre, KMITL)
22. Energy Dispersive X-ray Spectroscopy (OXFORD Instrument, X-Max^N, College of Advanced Manufacturing Innovation, KMITL)

3.3 Experimental procedure

3.3.1 Preparation of nickel pyrophosphate ($Ni_2P_4O_{12}$) supported on TiO_2 (P25) and SiO_2

10.0 wt.% of $Ni_2P_4O_{12}$ supported on TiO_2 (P25) and SiO_2 were prepared by incipient wetness impregnation method. The solution of nickel phosphate was prepared by dissolving 1.96 g of nickel nitrate hexahydrate and 1.78 g of ammonium phosphate (P/Ni = 2.0) in 17 mL of distilled water. 1 M of nitric acid was added dropwise to make the solution clear. After that, this solution was impregnated on 4.50 g of TiO_2-P25 or SiO_2 supports. The obtained samples were dried in the oven at 70 °C for 24 h and calcined in a muffle furnace at 500 °C for 6 h with the heating rate of 5 °C/min. The catalysts with P/Ni molar ratio of 0.5 were prepared similarly.

3.3.2 Preparation of nickel phosphide (Ni_2P) supported on TiO_2 (P25) and SiO_2 catalysts

To obtain Ni_2P catalysts, the prepared 10 wt.% $Ni_2P_4O_{12}$ supported on TiO_2 (P25), and SiO_2 samples were reduced to Ni_2P under H_2 at 650 °C. The schematic of reduction system is shown in **Figure 3.1**. The $Ni_2P_4O_{12}$ samples were ground and pelletized with a press and sieved to particles of 600- 850 μm diameter (20/40 mesh). Then, samples were reduced under H_2 (120 mL/min) at 650 °C for 0.5, 1 and 2 h with a heating rate 5 °C/min. After that, catalyst was cool down to room temperature under N_2 flow (25.0 mL/min) and then passivated at room temperature with O_2 flow 30.0 mL/min for 15 min.

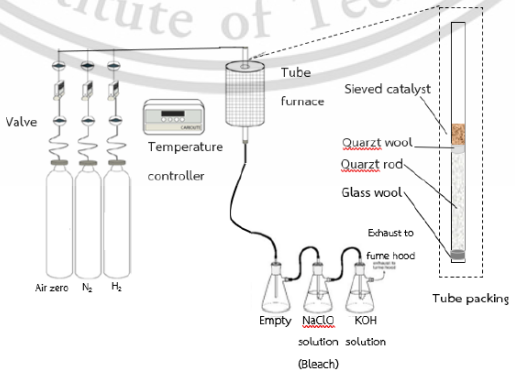

Figure 3.1. The schematic reduction rig for nickel phosphide preparation.

3.4 Characterization of catalyst on supports

3.4.1 X-ray Absorption Near Edge Structure (XANES)

The oxidation state and species of catalysts were evaluated using Synchrotron beam. A 25 mg of calcined sample was weighted and pressed with a 5 mm diameter mold followed by placing into the sample holder. The *in-situ* experimental for reduction was operated by temperature-programming from 50-650 ℃ (5 ℃/min) under a flow of 10% H_2 (30 mL/min) and held at 650 ℃ for 5 h after that cooldown under N_2 flow (30 mL/min) to room temperature. In addition, the tasted of water tolerant was operated by temperature-programming from 50-650 ℃ (10 ℃/min) under a flow of 10% H_2 (30 mL/min) and held at 650 ℃ for 30 min and cooldown again to room temperature. Then, ~5%moisture gas with temperature-programming from 50-700 ℃ (10 ℃/min) and held at 700 ℃ for 3 h. The XANES spectrum was collected for every 10 ℃ interval during the ramping and every 5 min interval during the holding at 650 ℃.

3.4.2 Brunauer-Emmett-Teller (BET) Surface area analysis

Surface area of catalysts will be determined using gas adsorption technique. The sample will be weighed (40-50 mg) and loaded into a cleaned and dried sample cell. After that, the sample will be degassed at 350 ˚C for 24 hours. The sample cell will be then removed from the out-gassing station after filling up with nitrogen and will be attached to the analysis station. The adsorption isotherm will be measured in a pressure range of 0.05-0.30 P/P_0 at -196 ˚C.

3.4.3 X-ray Fluorescence (XRF)

The chemical composition of a catalyst was analyzed by a wavelength-dispersive X-ray fluorescence spectrophotometer (WD-XRF), Bruker, Tiger. Approximately 0.5 g of a catalyst was mixed with 4.5 g of boric acid. The mixture was then manually grinded and compressed into a pellet. The data was recorded by X-ray source and quantitative calculated by theoretical formulas.

3.4.4 X-Ray Diffraction (XRD)

X-ray diffraction (XRD) for Nickel Phosphide catalyst on supports were performed using X-ray Diffractometer and X-ray Diffractometer, Shimadzu model XRD-6100 and Cu radiation. The sample was prepared by packing the pellets into the sample holder. The sample was scanned over the angle ranged from 2θ = 10.0-80.0,

40.0 kV and 30 mA. X-ray Diffraction pattern of the sample was compared with the X-ray Diffraction pattern of standard Nickel Phosphide catalyst for structure determination.

3.4.5 ^{31}P Magic angle spinning nuclear magnetic resonance (^{31}P MAS-NMR),

Solid ^{31}P magic angle spinning nuclear magnetic resonance spectra (^{31}P MAS-NMR) were recorded using a JEOL Resonance JNM-ECZ400R spectrometer (400MHz). Roughly 100 mg of sample was loaded into the spinner. The spinning rate during the measurement was 10 KHz.

3.5 Catalytic activity testing

The catalyst was sieved into particle size of 600-850 μm. After that, it was packed into the middle of a quartz tube reactor covered with quartz wool, filled quartz beads until it equal with 5 cm and packed quartz rods. The schematic of ethane steam cracking testing system is shown in **Figure 3.2**. The reactor was located at the center of a vertical tube furnace. Nitrogen was used as a makeup gas for injection to online-GC. The flow rate of the gases was controlled by a mass flow controller and checked by a bubble flow meter. Before activity testing, the nickel phosphide catalyst will be reduced under H_2 (110 mL/min) at 650 ˚C (rate 10 ˚C/min) for 30 min. Then steam and ethane was co-feed into the reactor by a syringe pumps and mass flow controller at the flow rate 5.9 mL/h and 24.58 mL/min, respectively. The catalytic testing was conducted for a total time on stream (TOS) of 3.5 h. The products were detected in two parts. First, light hydrocarbon which is non-condense products were detected by online-GC with HP-Plot column (condition is shown in **Table B1**). Second liquid products and water were trapped in 2 dodecane traps. After finishing the reaction, heavy oil was kept into volumetric flask (25 mL) which was consisted of cyclohexane 1 μL (internal standard) and dodecane in the total volume of 25 mL. The homogeneous sample was manual injected to GC (MTX-1 column) by using 10 μL syringe.

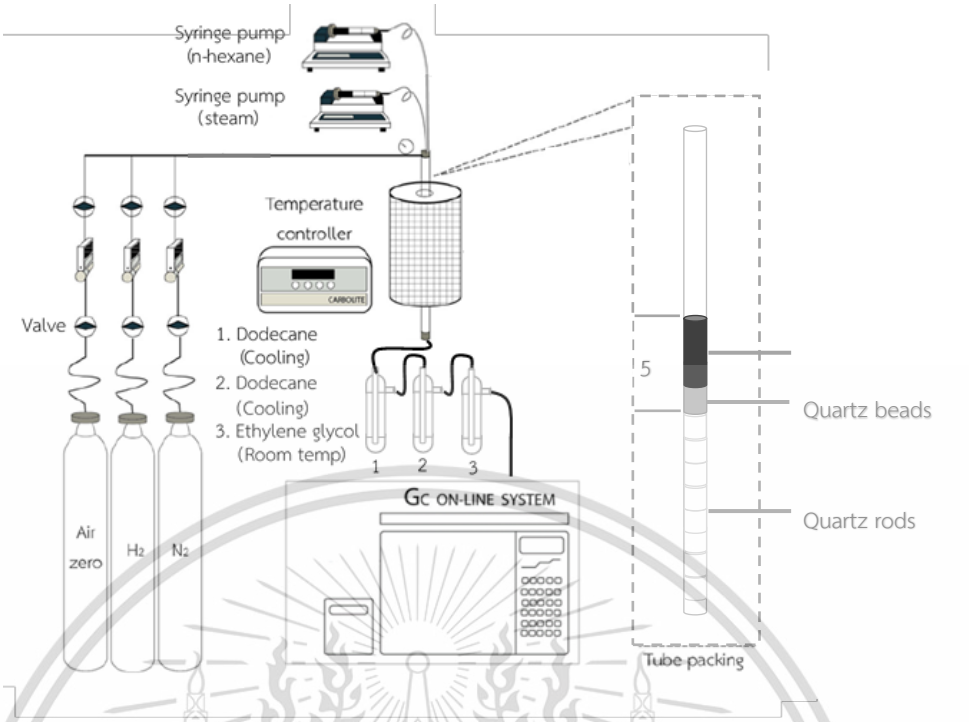

Figure 3.2. Schematic of catalytic testing reactor

CHAPTER 4
RESULTS AND DISCUSSION

4.1 Catalyst Characterization

The XRD spectrum of Ni_xP_y/TiO_2-0.5P prepared by P/Ni ratio of 0.5 showed the mixture Ni_2P and $Ni_{12}P_5$ species, where the peaks at 40.8°, 44.5°, 47.5° and 54.5° were ascribed to Ni_2P and the peaks at 38.7°, 41.9°, 47.1° and 48.8° were corresponded to $Ni_{12}P_5$ species (**Figure 4.1a**) [25]. On the other hand, Ni_2P/TiO_2-2.0P prepared by the excess phosphorus amount (P/Ni = 2.0) showed only Ni_2P species (**Figure 4.1b**). This indicates that the ratio of P/Ni plays an important role to form the nickel phosphide species. It had been reported in the literature that the excess of phosphorus was required in order to obtain pure Ni_2P since some of phosphorus would be lost as a PH_3 during the reduction step [62]. Accordingly, the preparation using the theoretical Ni_2P molar ratio (P/Ni = 0.5) would result in the deficient phosphorus to form Ni_2P but it would rather yield the $Ni_{12}P_5$ species as a mixture. In similar manner, Oyama *et al.,* reported that the pure Ni_2P phase over silica would be obtained when prepared by P/Ni = 0.5 [25]. Furthermore, Hua *et al.*, reported that the P/Ni <1 would be required for the supported Ni_2P over MCM-41 (Ni_2P/MCM-41) [63].

In line with the XRD results, only Ni_2P species in Ni_2P/TiO_2-2.0P was detected by the ^{31}P MAS NMR spectroscopy (**Figure 4.2b**, singlet peaks at 4050 and peaks at ~1500 ppm with the side band [64]). Whereas the additional peaks at 1934 ppm and 2262 ppm corresponding to $Ni_{12}P_5$ species were observed in Ni_xP_y/TiO_2-0.5P (**Figure 4.2a**) [64]. In addition, these two samples show the peak at 0 ppm which is ascribe to the PO_4^{3-} species, similarly to those of $Ni_2P_4O_{12}/TiO_2$-2.0P – the parent sample. This remaining PO_4^{3-} after the reduction emphasizes that not all phosphorus would be reduced to form nickel phosphide species. According the excess phosphorus during the synthesis would be required. It is worth nothing that despite the different nickel phosphide species obtained in these two samples, the Ni content (~7 wt.% loading) determined by XRF (**Table 4.1**) for both samples are similar.

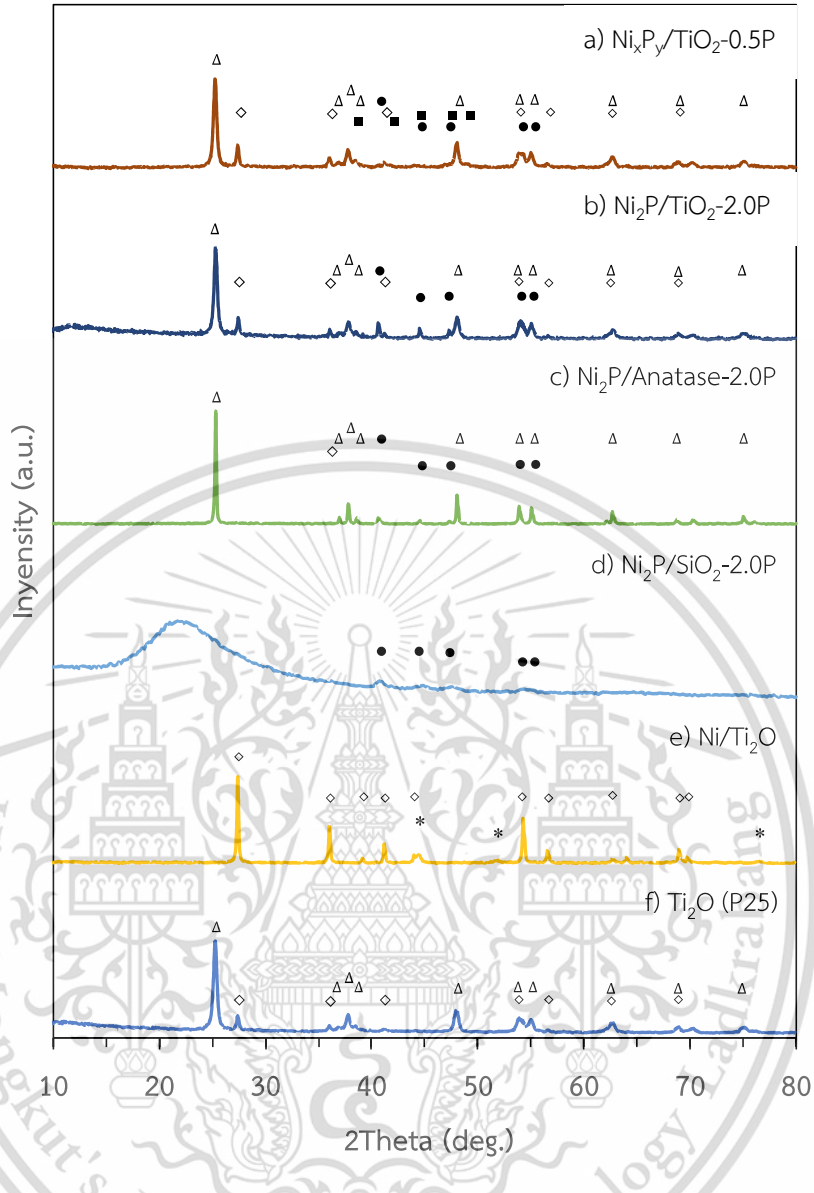

Figure 4.1 XRD pattern of all samples (△ Anatase, ◊ Rutile, ● Ni_2P, ■ $Ni_{12}P_5$, ∗ Ni, and ★ $NiTiO_3$).

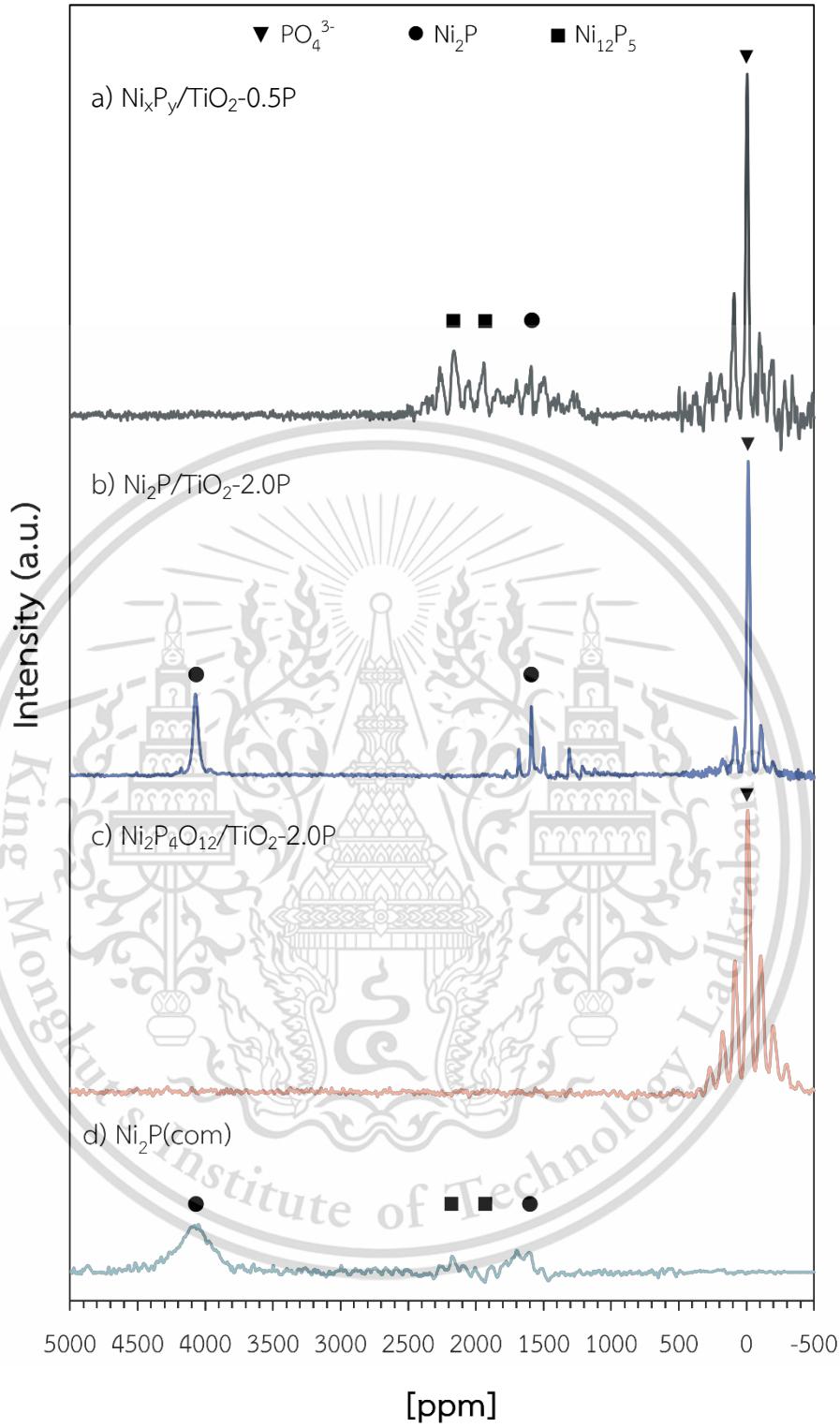

Figure 4.2 ^{31}P MAS NMR spectra of catalysts with different synthesized methods, catalysts precursor and commercial nickel phosphide (Ni_2P) (▼ PO_4^{3-}, ● Ni_2P, ■ $Ni_{12}P_5$).

Considering the TiO_2 support, both rutile and anatase XRD characteristic peaks in Ni_xP_y/TiO_2-0.5P and Ni_2P/TiO_2-2.0P remains the same, as compared to their parent support (**Figure 4.1h**, rutile: 2θ at 26°, 35°, 39°, 53°, 55°, 60° and 65°, anatase: 2θ at 25°, 39°, 48°, 54°, 55° and 61°). This suggests that the reduction treatment at 650 °C under H_2 for 2 h to prepare the supported Ni_2P catalysts, does not affect the crystallinity of the TiO_2(P25). In sharp contrast, only rutile characteristic peaks were observed in Ni/TiO_2, indicating the transformation of anatase phase to rutile phase in this sample under the similar preparation (calcination 500 °C and reduction at 650 °C). It is well-known that TiO_2(P25) can change the phase from anatase to rutile at temperature >550 °C. Xu *et al.*, suggested that upon the calcination at ≥550 °C, the nickel dopped on TiO_2(P25) could cause the oxygen vacancies leading to the substitution Ti^{4+} by Ni^{2+}, causing the expansion in a (= b) plane and decrease in c plane [65]. This results in the change in crystallinity from anatase to rutile phase [65]. Accordingly, under the reduction atmosphere, metallic Ni in Ni/TiO_2 could promote the generation of oxygen vacancy over the TiO_2, resulting in the phase transformation of the TiO_2(P25) to TiO_2(rutile) [66]. However, the phase transformation was not observed in Ni_xP_y/TiO_2-0.5P and Ni_2P/TiO_2-2.0P samples. This could be attributed to the presence of phosphorus inhibiting the phase transformation due to the existence of TiP_2O_7 species as reported by Gopal *et al.*,[67]. In a supportive manner, the TiO_2(P25) phases in $Ni_2P_4O_{12}/TiO_2$-2.0P (parent sample of Ni_2P/TiO_2-2.0P) remained the same.

Table 4.1 The specific surface area, elemental composition[a], and Ni_2P crystallite size[b] of catalysts

Entry	Sample	Elemental composition (wt.%)		S_{BET} (m^2/g)	Ni_2P Crystallite Size (nm)
		Ni	P		
1	Ni_xP_y/TiO_2-0.5P	7.7	1.8	38	33.7
2	Ni_2P/TiO_2-2.0P	7.0	5.4	42	31.2
3	Ni_2P/TiO_2(anatase)-2.0P	6.8	1.3	17	42.8
4	Ni_2P/SiO_2-2.0P	7.7	3.1	214	44.0
5	Ni/TiO_2	9.6	-	46	-

[a] Determined by XRF

[b] Determined by XRD ; Ni_2P crystallite size of Ni_2P/TiO_2(Phy) = 52.7 nm

The difference in Ni species of Ni_xP_y/TiO_2-0.5P and Ni_2P/TiO_2-2.0P samples was also evidenced in *in-situ* X-ray near edge structure spectroscopy (*in-situ* XANES). The XANES spectra and the Ni K-edge energy (8332.89 eV) of Ni/TiO_2 are similar to those of metallic Ni standard (**Figure 4.3b**, **Table 4.2**). On the other hand, the *in-situ* XANES line-shape spectra of Ni_xP_y/TiO_2-0.5P and Ni_2P/TiO_2-2.0P are more resemble to Ni_2P(com). Furthermore, the Ni K-edge energy of these nickel phosphides samples (8336-8337 eV, **Table 4.2**) are higher than the metallic Ni (8332.89 eV) due to their lower electron density. In addition to those, Ni_2P/TiO_2-2.0P has the same Ni K-edge energy to Ni_2P(com) (8337.05 eV, **Table 4.2**). This emphasizes the presence of Ni_2P species in this sample. While, Ni_xP_y/TiO_2-0.5P has a slightly lower Ni K-edge energy (8336.53 eV), indicating a slightly higher electron density. This could be attributed to the presence $Ni_{12}P_5$ – a higher electron density Ni phosphide species – in Ni_xP_y/TiO_2-0.5P, as previously evidenced in the XRD and NMR results [68].

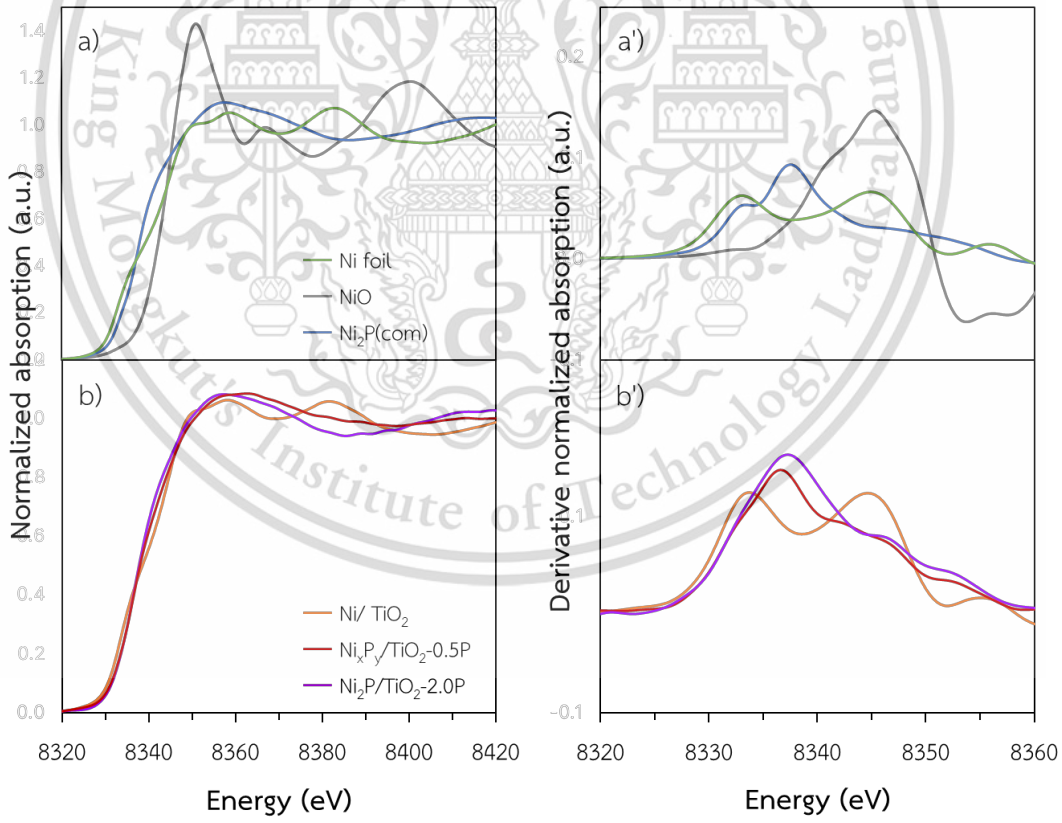

Figure 4.3 Nickel K-edge XANES spectra of Ni_xP_y/TiO_2-0.5P, Ni_2P/TiO_2-2.0P, Ni/TiO_2, and standards (Ni foil, NiO, and Ni_2P).

Table 4.2 The fraction of Ni species in Ni_xP_y/TiO_2-0.5P and Ni_2P/TiO_2-2.0P catalysts

Entry	Sample	K-edge energy (eV)	Fraction (%)		
			Ni^{2+}	Ni^{n+}	Ni^0
1	Ni_xP_y/TiO_2-0.5P	8,336.53	0	78.5	21.5
2	Ni_2P/TiO_2-2.0P	8,337.19	0	100	0
3	Ni/TiO_2	8,333.70	0	0	100
4	Ni foil	8,332.89	-	-	100
5	NiO	8,345.28	100	-	-
6	Ni_2P(com)	8,337.05	-	100	-

Ni^{n+} using Ni_2P as a reference ($0 < n < 2$).

The linear combination of *in-situ* XANES using NiO as a standard for Ni^{2+}, Ni foil for Ni^0, and Ni_2P for nickel phosphide are summarized in **Table 4.2**. It can be seen that the Ni species in Ni_2P/TiO_2-2.0P is only Ni_2P indicating the pure Ni_2P over this sample as previously discussed. While, the Ni_xP_y/TiO_2-0.5P has the mixture of Ni_2P (78.5%) and Ni^0 (21.5%). Though, none of the metallic phase was detected in the XRD suggesting the highly dispersed Ni particle over this sample. It is worth noting that as no standard $Ni_{12}P_5$ is available, the amount of Ni_2P species from linear combination could be represent both $Ni_{12}P_5$ and Ni_2P. For Ni/TiO_2, only metallic Ni species are obtained.

Since the nickel phosphide species obtained from different P/Ni ratio used during the preparation are different, the formation of the nickel phosphide upon the reduction was thus further evaluated in the *in-situ* TR-XANES, as compared to the supported Ni catalyst. The results are shown in **Figure 4.4**.

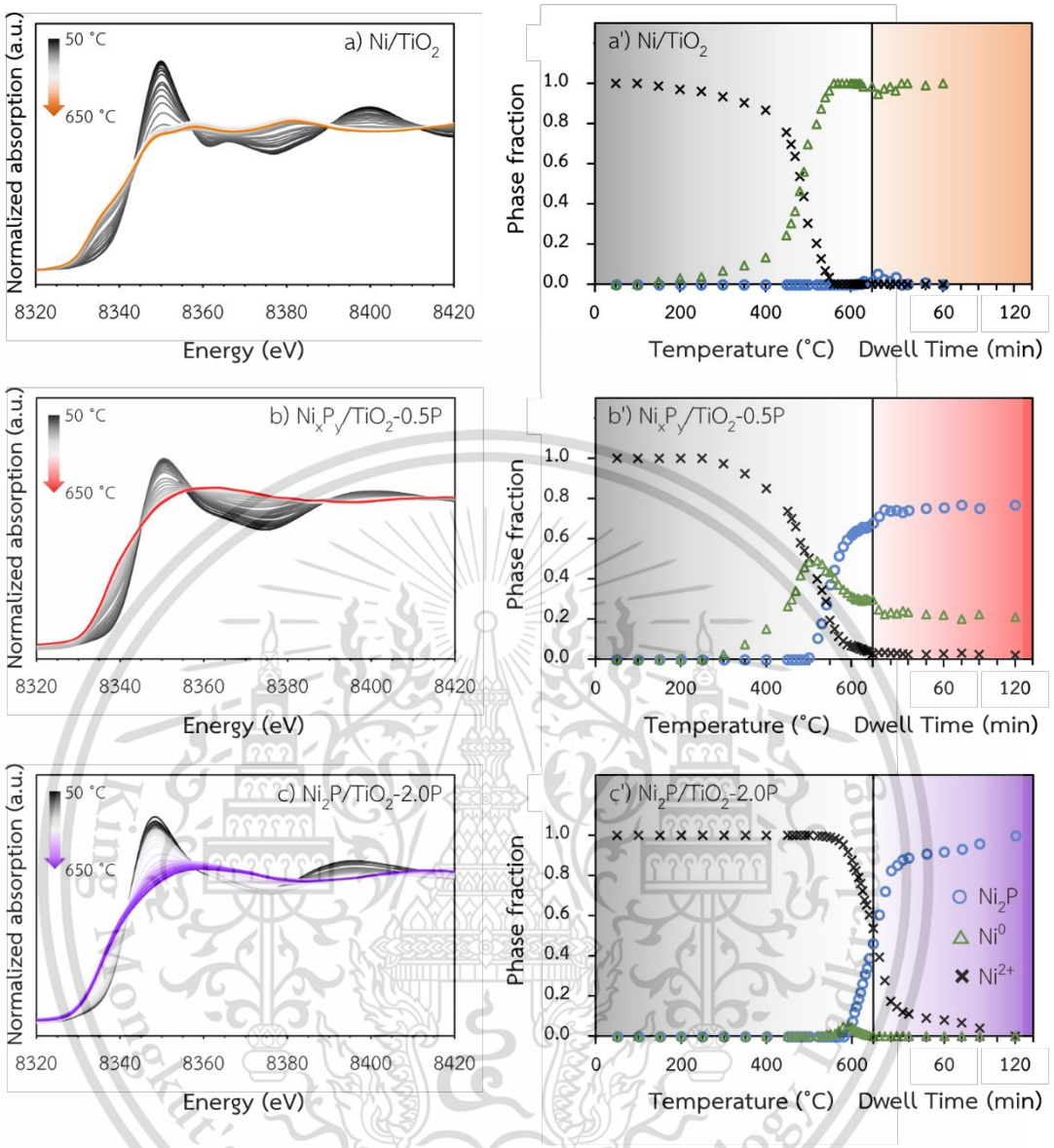

Figure 4.4 Spectra of the *in-situ* time-resolved X-ray absorption near-edge structure spectroscopy (*in-situ* TR-XANES) of Ni/TiO_2 (a), Ni_xP_y/TiO_2-0.5P (b), and Ni_2P/TiO_2-2.0P (c) samples and the fraction of Ni species from linear combination fitting of Ni/TiO_2 (a'), Ni_xP_y/TiO_2-0.5P (b'), and Ni_2P/TiO_2-2.0P (c') samples under reduction condition from 50 to 650 °C with holding at 650 °C for 60-120 min using Ni foil (△), NiO (×), and Ni_2P (○) standards.

It can be seen in **Figure 4.4a and a'** that the Ni^{2+} species in Ni/TiO_2 initially started to reduce to metallic Ni (Ni^0) at 150 °C and fully reduced at 550 °C. It is possible that the reduction of Ni^{2+} at low temperature (<300 °C) could be attributed to the reduction at the surface of bulk NiO particles. While the reduction at the temperature

above 300 °C could be contributed to the $NiTiO_3$ species that have a strong metal-support interaction as typically observed in the literature [69]. It is noted that the reduction rate is relatively fast at 450-550 °C.

In sharp contrast, the reduction of Ni^{2+} over Ni_xP_y/TiO_2-0.5P and Ni_2P/TiO_2-2.0P was observed at a higher temperature, as compared to Ni/TiO_2 (**Figure 4.4**). For Ni_xP_y/TiO_2-0.5P, the metallic Ni was initially obtained at 300 °C and continuously increased to ~46% Ni^0 at 490 °C. This could be attributed to the highly dispersed NiO species that has the strong interaction with the support. During the preparation with half a molar of $(NH_4)_2(HPO_4)$ compared with $Ni(NO_3)_2$, the mixture of $NiNH_4PO_4$ and NiO could be formed, as shown in **Equation 1**. Furthermore, some of NiO species would be additionally formed from the $NiNH_4PO_4$ after the calcination at 500 °C, especially in the presence of NH_4NO_3 (**Equation 2**), as reported by Wang *et al.* [70]. This could lead to the higher dispersion of the NiO species. Moreover, the agglomeration of NiO could thus be suppressed by the presence of this phosphorus precursor, as also mentioned by Liu *et al.* [71].

$$2Ni(NO_3)_2 + (NH_4)_2HPO_4 \longrightarrow NiNH_4PO_4 + NiO + H_2O + NH_3 + 4NO_2 + O_2$$

Equation 1 The $NiNH_4PO_4$ and NiO formation via reaction of $Ni(NO_3)_2$ with $(NH_4)_2(HPO_4)$ precursor.

$$NiNH_4PO_4 \xrightarrow{350\text{-}500\ ^oC} NiO + NH_3 + 1/2\ P_2O_5 + 1/2\ H_2O$$

Equation 2 The NiO alternative formation from the direct decomposition of $NiNH_4PO_4$.

At the reduction temperature at 500 °C of Ni_xP_y/TiO_2-0.5P, Ni_2P species was initially observed (0.1%) as a mixture with metallic Ni (50%, **Figure 4.4b**). The formation of Ni_2P continuously increased to 79% after reduction at 650 °C for 2 h, while the metallic Ni species decreased to 29%. This evidence clearly suggests that the Ni metallic was initially formed, which could be then transformed to Ni_2P by reacting with phosphorus produced from the reduction of phosphate (PO_4^{3-}), as mentioned in the literature (**Equation 3**) [64, 68, 72, 73]. In a supportive manner, Stinner *et al.* had

proposed that the metallic Ni could catalyze the reduction of the phosphate to form reactive P species, such as PH_3 and P, [64], presumably via the hydrogen spillover [74, 75]. Subsequently the P species would react with Ni atoms to form the Ni_2P species as shown in **Equation 4** [64].

$$P_2O_5 + 8H_2 \longrightarrow 2PH_3 + 5H_2O \longrightarrow 2P + 3H_2 + 5H_2O$$

Equation 3 The reduction of P_2O_5 to produce PH_3 and P.

$$2Ni + P \longrightarrow Ni_2P$$

Equation 4 The formation of Ni_2P from the reaction between Ni and P.

It is worth to note that not all of metallic Ni species in Ni_xP_y/TiO_2-0.5P would transform to Ni_2P (**Figure 4.4b**). This could be attributed to the insufficient phosphorus to react with the metallic Ni. It is possible that the phosphate species might not be all reduced. In fact, some of PO_4^{3-} would still remain, as evidence by ^{31}P MAS NMR (**Figure 4.2**). Furthermore, some of the phosphine (PH_3) formed during the reduction could be lost since it is volatile. Alternatively, the formation of a Ni-rich metal phosphide ($Ni_{12}P_5$) could be obtained presumably via the reaction between metallic Ni and Ni_2P (**Equation 5**), as evidenced by XRD, ^{31}P MAS NMR results and discussed earlier. Thus, the use of low phosphorus precursor as compared to the Ni would tend to yield the mixture of nickel phosphides, as also reported in the literature [72, 76].

$$2Ni + 5Ni_2P \longrightarrow Ni_{12}P_5$$

Equation 5 The possible partway of $Ni_{12}P_5$ formation.

In sharp contrast, the reduction Ni^{2+} species in the Ni_2P/TiO_2-2.0P prepared by the excess phosphorus (P/Ni = 2.0), was at a much higher temperature (>520 ˚C), as compared to others. According to the linear combination fitting in **Figure 4.4c'**, the metallic Ni species was started to observe at 520 ˚C for 0.1% and increased to 5.2% at 590 ˚C. Such very high reduction temperature could be attributed to the reduction of $Ni_2P_4O_{12}$ species to the metallic Ni species (**Equation 6**). Under the excess phosphorous environment, Wang *et at.* mentioned that $NiNH_4PO_4$ could be only form

without the NiO (**Equation 7**) [70]. Furthermore, the excessive remaining $NH_4H_2PO_4$ could be decomposed to P_2O_5 at >350 ˚C, as shown in **Equation 8**. Under calcination at 500 ˚C, $Ni_2P_4O_{12}$ could be yielded from the reaction between $NiNH_4PO_4$ and P_2O_5 (**Equation 9**).

$$Ni_2P_4O_{12} + 36H_2 \longrightarrow 2Ni + 4PH_3 + 12H_2O$$

Equation 6 The metallic Ni formation from the reduction of $Ni_2P_4O_{12}$.

$$Ni(NO_3)_2 + (NH_4)_2HPO_4 \longrightarrow NiNH_4PO_4 + NH_4NO_3 + 1/2H_2O + NO_2 + 1/4O_2$$

Equation 7 The $NiNH_4PO_4$ formation via reaction of $Ni(NO_3)_2$ with $(NH_4)_2(HPO_4)$ precursor.

$$2NH_4H_2PO_4 \xrightarrow{350\text{-}500\ ^oC} P_2O_5 + 2NH_3 + 3H_2O$$

Equation 8 The decomposition of $NiNH_4PO_4$ to produce P_2O_5.

$$2NiNH_4PO_4 + P_2O_5 \xrightarrow{350\text{-}500\ ^oC} Ni_2P_4O_{12} + 2NH_3 + H_2O$$

Equation 9 The $Ni_2P_4O_{12}$ formation from the reaction of $NiNH_4PO_4$ with P_2O_5.

Interestingly, the formation of Ni_2P species in Ni_2P/TiO_2-2.0P was at higher temperature than Ni_xP_y/TiO_2-0.5P. According to **Figure 4.4c'**, Ni_2P species was initially evidenced at 590 ˚C which was right after the metallic Ni formed. As the temperature increases, the formation of the Ni_2P was then rapidly with only trace amount of metallic Ni. It is possible that Ni preliminary formed could promptly react with phosphorous to form Ni_2P for the excess phosphorous methodology. In fact, none of metallic Ni species was observed after reduction at 650 ˚C for 2 h and only Ni_2P species was obtained in Ni_2P/TiO_2-2.0P. According to literature, the reduction of $Ni_2P_4O_{12}$ to Ni_2P could be readily at 650 ˚C (**Equation 10**). In addition to this, the *in-situ* TR-XANES could suggest that the metallic Ni could catalyze the reduction of $Ni_2P_4O_{12}$ to Ni_2P since the metallic Ni was initially observed prior the formation of Ni_2P. However, the formation of Ni_2P in the 2.0P method requires higher temperature due to the different source of Ni precursor ($Ni_2P_4O_{12}$ for 2.0P and NiO for 0.5P). It is noted that for

preparation by 0.5P method, $Ni_2P_4O_{12}$ could also be formed since there are some trace amounts of P_2O_5, presumably from i) the calcination of $NiNH_4PO_4$ to NiO step and ii) the decomposition of unreacted $NH_4H_2PO_4$.

$$Ni_2P_4O_{12} + 15H_2 \longrightarrow Ni_2P + 3PH_3 + 12H_2O$$

Equation 10 The formation of Ni_2P from the reduction of $Ni_2P_4O_{12}$.

Upon using excess phosphorous method, pure N_2P species were also obtained for N_2P/SiO_2 and Ni_2P/TiO_2(anatase) similarly method as Ni_2P/TiO_2-2.0P. Only Ni_2P species were detected in the XRD of N_2P/SiO_2 and Ni_2P/TiO_2(anatase) (**Figure 4.1c** and **d**). This emphasizes that the excess phosphorous as compared to Ni is required to synthesize the Ni_2P despite the different in surface area and acidity/basicity of the support. In line with this view, pure Ni_2P supported on MCM41, fume silica, ZSM-5, carbon nanotube, alumina and zirconia was successfully obtained by preparation of excess phosphorous (P/Ni > 1). [73, 77-80].

4.2 Catalytic steam cracking of ethane

The catalytic activity of Ni_2P catalysts towards steam cracking of ethane was evaluated in the continuous fixed-bed reactor at 650˚C under atmospheric pressure. The results are summarized in **Table 4.3**. Ni_2P/TiO_2-2.0P, possessing pure Ni_2P species, yielded 99.0% ethylene selectivity with the ethane conversion rate of 65.2 $mmol_{ethylene}.g_{Ni}^{-1}.h^{-1}$. In fact, ethylene productivity is 64.6 $mmol_{ethylene}.g_{Ni}^{-1}.h^{-1}$. This suggests that Ni_2P species is selective towards the C-H cracking. This is in consistent with the computation results reported by Jeonghyun *et al.* that the nickel phosphide (Ni_2P) would facilitate the C-H bond breaking of ethane where ethyl group would be adsorbed at the P site (P1, **Scheme 4.1**) and hydrogen would be interact with the neighboring fcc Ni hold site (M3, **Scheme 4.1**) on $Ni_2P(001)$ [81]. In addition, they mentioned that the desorption of ethylene over the Ni_2P (001) could be more facile than over the Ni (111) due to a poorer affinity of the Ni_2P. In addition, Schneider *et al.* suggested that the further dehydrogenation of ethylene was less facile over the Ni_2P than Ni since the alkyl intermediates tend to bind with the P sites.

Table 4.3 Catalysts activity at time on stream 210 min

Entry	Catalyst	Rate ($mmol_{ethane}.g_{Ni}^{-1}.h^{-1}$)	Productivity ($mmol.g_{Ni}^{-1}.h^{-1}$)		Selectivity (%Yield)			
			Ethylene	Methane	Ethylene	Methane	Coke	Syn gas
1	Ni_2P/TiO_2-2.0P	65.2	64.6	1.2	99.0	1.0	0.0	0.0
2	Ni/TiO_2	1431	0.0	254.5	0.0	8.9	11.1	80.0
3	Ni_xP_y /TiO_2-0.5P	43.5	31.4	1.1	72.2	1.1	0.6	26.1
4	Ni_2P/TiO_2(anatase)-2.0P	25.9	25.1	0.0	96.4	0.0	3.6	0.0
5	Ni_2P/SiO_2-2.0P	21.6	21.6	0.0	100	0.0	0.0	0.0
6	Ni_2P/TiO_2(Phy)	27.2	27.2	0.0	100	0.0	0.0	0.0

Reaction condition: T_{react} *= 650 ℃,* F_{Ethane} *= 24.6 mL/min (99.95%), W/F = 7.3* $g_{catalyst}{\cdot}h{\cdot}mol_{Ethane}^{-1}$*, atmospheric pressure. The values shown were taken at 210 minutes time on stream.*

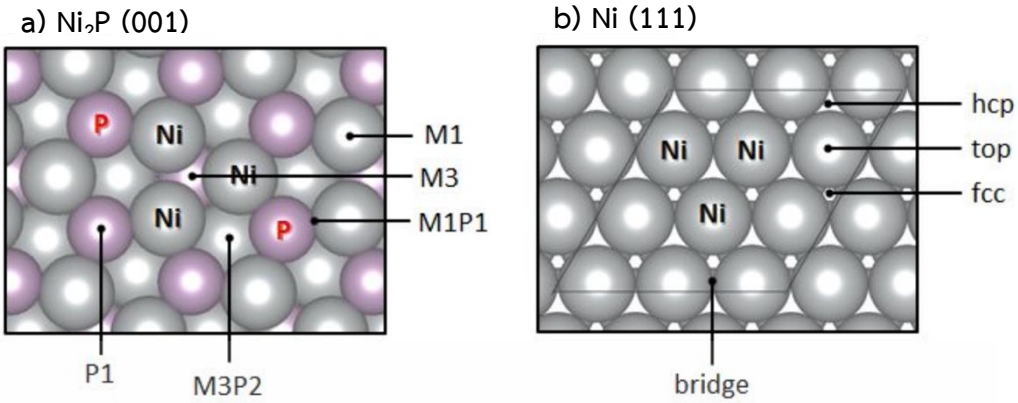

Scheme 4.1. Top views of a) A-termination of $Ni_2P(001)$ and b) the Ni(111). Computational supercells are indicated with light lines, Ni atoms shown in gray, P in purple, and adsorption sites labeled on each surface.

It is interesting that Ni_2P/TiO_2-2.0P yielded only trace amount of methane (~1% selectivity), presumably from the hydrogenolysis. While none of coke and syn gas were observed. This could suggest that Ni_2P would be less active toward the C-C breaking unlike the metallic Ni. In a supportive manner, Ni/TiO_2 provided mainly syn gas (~80) and methane (~9%), presumably from ethane steam reforming and hydrogenolysis, respectively. In fact, the very high ethane conversion rate (1431 $mmol_{ethane} \cdot g_{Ni}^{-1} \cdot h^{-1}$) was obtained from this catalyst. This clearly indicates that the C-C breaking is more readily over the metallic Ni surface as compared to Ni_2P. Due to a greater affinity of Ni, the interaction between the C* or CH* with metallic Ni species is much greater than the Ni_2P [82]. Accordingly, a C-C activation would be more facile over the metallic Ni than the Ni_2P. This result is also consistence with Zhang *et al.* reporting that the steam reforming of propane over Ni/Al_2O_3 at 500 °C was achieved with syn gas, CO_2 and CH_4 products. The selectivity for syn gas, CO_2 and CH_4 would be 25%, 43% and 32%, respectively [83].

The ethylene productivity decreases by half once using Ni_xP_y/TiO_2-0.5P (31.4 $mmol_{ethane} \cdot g_{Ni}^{-1} \cdot h^{-1}$, **Table 4.3**), as compared to Ni_2P/TiO_2-2.0P (64.6 $mmol_{ehtylene} \cdot g_{Ni}^{-1} \cdot h^{-1}$). In addition, the ethane conversion rate decreased from 65.2 to 43.5 $mmol_{ethane} \cdot g_{Ni}^{-1} \cdot h^{-1}$. This could be attributed to the lower Ni_2P species over this samples since there is a mixture of Ni_2P and $Ni_{12}P_5$. In line with view, it has been reported by Zhu *et al*., in the literature that the $Ni_{12}P_5$ or mixture of $Ni_{12}P_5$ and Ni_2P provided a lower activity on dehydrogenation. This could be attributed to the low adsorption activity of the $N_{12}P_5$

[84]. Furthermore, syn gas (CO and H_2) and coke were observed for 26.1% and 0.6%, respectively. This could be attributed to the more metallic Ni species of $Ni_{12}P_5$, leading to a more facile of C-C breaking similarly to those of metallic Ni; however, they are less active.

The high ethylene selectivity (>96%, **Table 4.2**) was obtained from Ni_2P/TiO_2(anatase)-2.0P; however, the much lower ethane conversion rate was observed, as compared to Ni_2P/TiO_2-2.0P. This emphasizes that the Ni_2P species is active towards the ethane dehydrogenation since the Ni_2P species observed on both catalysts as discussed earlier. The observed lower activity could be attributed to the lower surface area of Ni_2P/TiO_2(anatase)-2.0P (17 m^2/g) than Ni_2P/TiO_2-2.0P (42 m^2/g). In turn, Ni_2P/SiO_2-2.0P possessing the high surface area (214 m^2/g) yielded even a lower the ethane conversion rate, as compared to the Ni_2P/TiO_2(anatase)-2.0P. Though, the high ethylene selectivity was retained. This suggests that the strong metal support interaction between Ni_2P and the TiO_2 plays an important role. To get more evidence, the physical mixing of Ni_2P and TiO_2 (Ni_2P/TiO_2(Phy)) was prepared and tested for the reaction. It is noted that the surface area of Ni_2P/TiO_2(Phy) is 47 m^2/g similarly to Ni_2P/TiO_2-2.0P. It can be seen in **Table 4.3 entry 6** that the ethane conversion rate is still lower than Ni_2P/TiO_2-2.0P. The high ethylene selectivity was still observed. Hence, this emphasizes that both surface area and SMSI play role on the catalytic activity similarly to those other supported metal as reported in the literature [85].

In line with those view, Ni_2P/TiO_2-2.0P initially yielded high ethylene selectivity (>99%) at relatively low *W/F* (3.6 $g_{catalyst}\cdot h\cdot mol_{Ethane}^{-1}$), as shown in **Figure 4.5**. In addition, the conversion rate gradually increases as the *W/F* enhance. Methane productivity was also inclined, especially at *W/F* >5.5 $g_{catalyst}\cdot h\cdot mol_{Ethane}^{-1}$. The increase in the activity could be mainly attributed to higher Ni_2P active sites. Furthermore, this results again emphasizes that Ni_2P species are very selective towards the C-H bond breaking.

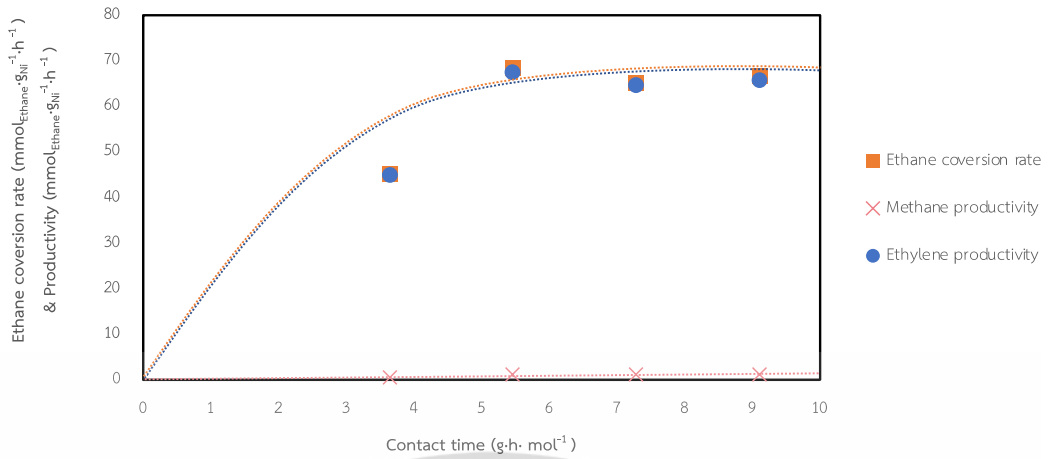

Figure 4.5 Conversion of ethane and yield of products over Ni_2P/TiO_2-2.0P catalyst. *Reaction condition*: T_{react} = 650 ℃, F_{Ethane} = 24.6 mL/min (99.95%), W/F = 7.3 $g_{catalyst}$·h·mol_{Ethane}^{-1}, atmospheric pressure. The values shown were taken at 210 minutes time on stream.

It is worth noting that upon performing the ethane steam cracking for 11 h using Ni_2P/TiO_2-2.0P as a catalyst, the product selectivity was changed, as shown in **Figure 4.6**. Ethylene selectivity was decreased from 100% to 95% over 11 h, while methane increased to 5% selectivity. This could be attributed to the transformation of Ni_2P to metallic Ni species. In line with this view, it can be seen that the ethane conversion rate increases from 28 $mmol_{Ethane}·g_{Ni}^{-1}·h^{-1}$ at 0.5 h to 65 $mmol_{Ethane}·g_{Ni}^{-1}·h^{-1}$ at 3.5 h which could be presumably due to the metallic Ni species that is more active towards C-C breaking. Though, it decreases to 42 $mmol_{Ethane}·g_{Ni}^{-1}·h^{-1}$ at 11 h. Though, this deactivation could be attributed to the coke formation. In line with this view, none of Ni_2P was observed in the XRD of used Ni_2P/TiO_2-2.0P for 11 h (**Figure 4.7**); while the NiO phase was detected. Furthermore, none of anatase phase was retained in this sample, indicating the presence of metallic Ni, as discussed earlier. This could indicate that the Ni_2P was changed to metallic Ni that could be oxidized to NiO.

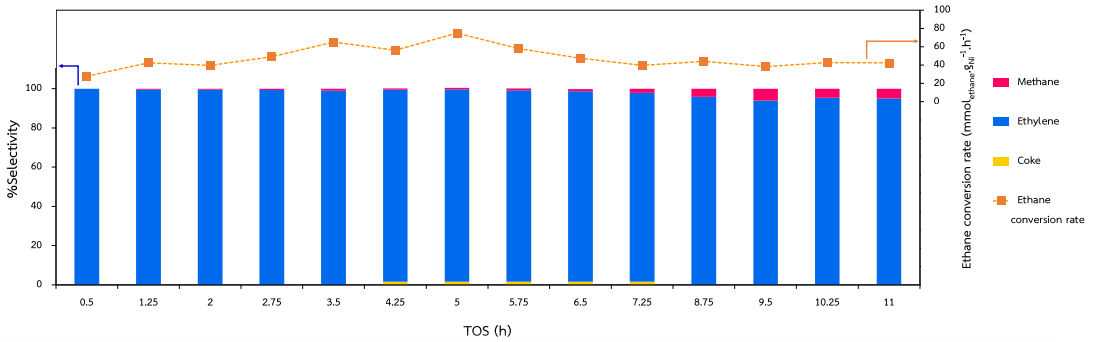

Figure 4.6 The selectivity of ethylene and methane from catalytic steam cracking of ethane over Ni_2P/TiO_2-2.0P at 30 min, 210 min and 660 min. *Reaction condition*: T_{react} = 650 °C, F_{Ethane} = 24.6 mL/min (99.95%), W/F = 7.3 $g_{catalyst}$·h·mol_{Ethane}^{-1}

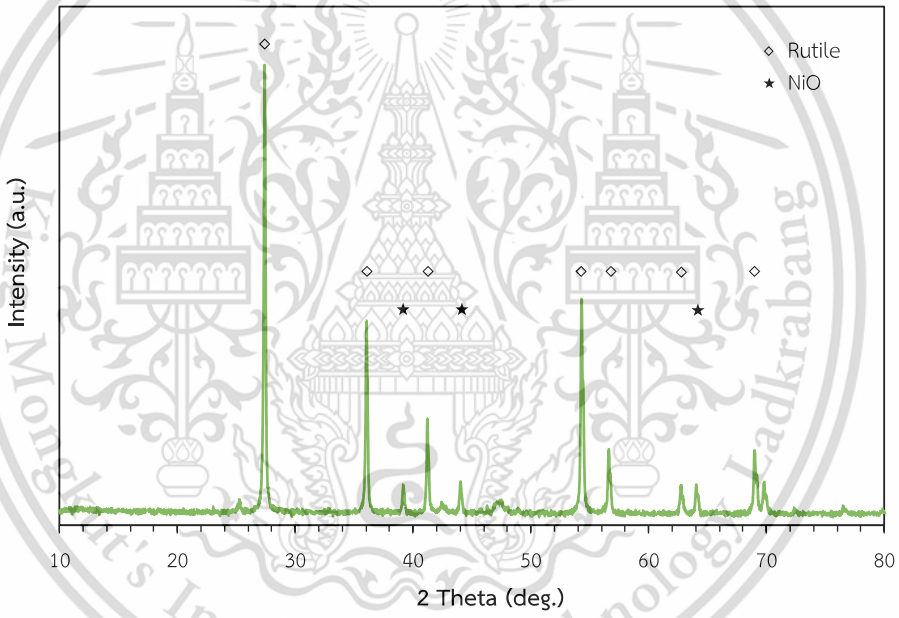

Figure 4.7 The XRD pattern of Ni_2P/TiO_2-2.0P at TOS 11 h.

To gain more evidence about the transformation of Ni_2P to metallic Ni, the reduction of Ni_2P/TiO_2-2.0P *in-situ* TR-XANE was performed under steam of H_2 at 650°C for 3 h. It can be clearly seen in **Figure 4.8a**, the white line intensity slightly decreases during time. The linear combination in **Figure 4.8b** shows the decrease in Ni_2P composition to 68.5% at 3 h, while the metallic Ni increases to 31.5%. This evidence clearly indicates the transformation of Ni_2P to Ni^0. It is possible that the Ni_2P was

reduced to metallic Ni and PH_3/Phosphorous. Even though the Ni_2P over TiO_2 is very selective to produce ethylene from ethane steam cracking, its stability due to the change in the species needs to be improved.

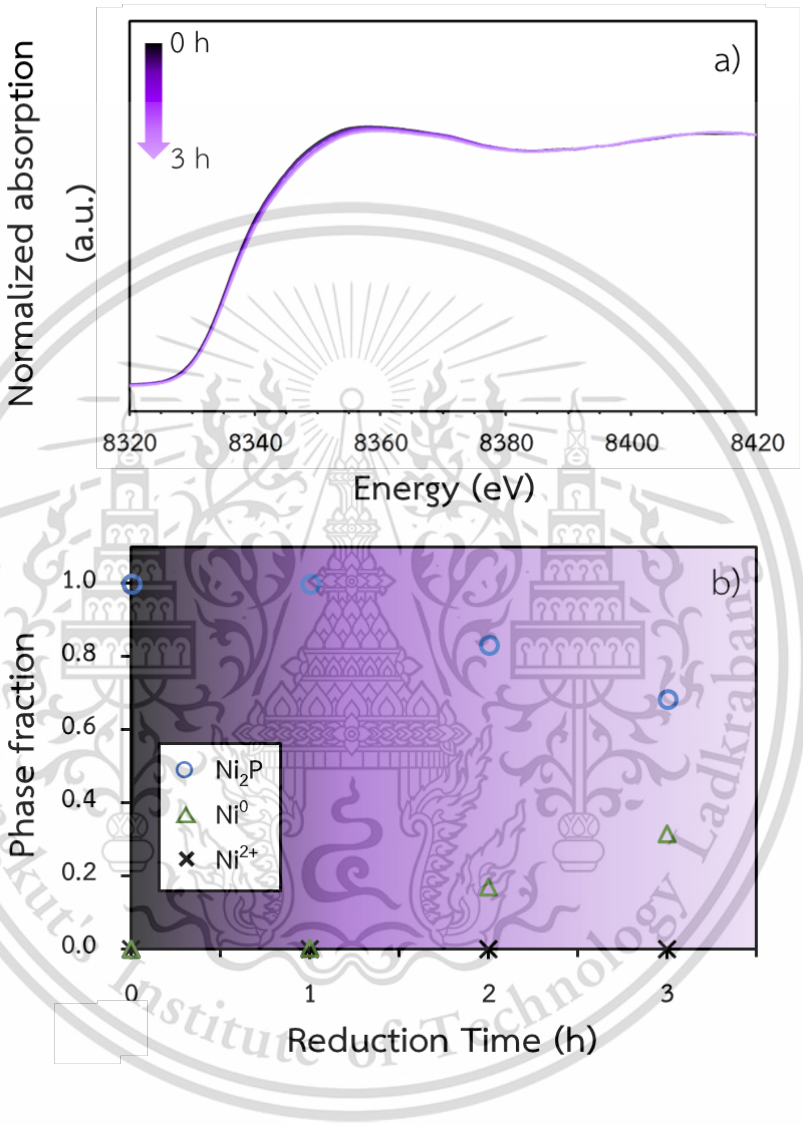

Figure 4.8 Spectra of the *in-situ* time-resolved X-ray absorption near-edge structure spectroscopy (*in-situ* TR-XANES) of Ni_2P/TiO_2-2.0P under reduction condition at 650 °C for 300 min using Ni foil (△), NiO (×), and Ni_2P (○) standards.

CHAPTER 5
CONCLUSIONS AND SUGGESTIONS

5.1 Conclusions

The formation of Ni_2P over a support (TiO_2 and SiO_2) using different P/Ni molar ratio (0.5 and 2.0) for the preparation was studied and the prepared Ni_2P samples were tested as a catalyst for ethane steam cracking. For Ni_xP_y/TiO_2-0.5P prepared by P/Ni molar ratio of 0.5, the mixture of Ni_2P and $Ni_{12}P_5$ species was observed by XRD and ^{31}P MASNMR. The *in-situ* XANES suggested that the formation of Ni_2P over this synthesis method was preliminarily involved in the reduction of NiO species to metallic Ni that was then react with the phosphorous to form nickel phosphide species. However, the limitation of phosphorous leads to the mixture of Ni_2P and $N_{12}P_5$ species. In sharp contrast, under excess phosphate precursor (P/Ni molar ration of 2.0) for Ni_2P/TiO_2-2.0P, pure Ni_2P was obtained as evidenced by XRD, ^{31}P MASNMR, and *in-situ* XANES. Furthermore, the formation of Ni_2P was observed under a much higher temperature, as compared to Ni_2P/TiO_2-2.0. This could be due to the reduction of $Ni_2P_4O_{12}$ to the metallic Ni species. Once the metallic Ni formed, the formation of Ni_2P was relatively fast suggesting that the metallic Ni could catalyze the reduction of $Ni_2P_4O_{12}$ to Ni_2P. Upon using excess phosphorous method, pure N_2P species were also obtained for N_2P/SiO_2 and Ni_2P/TiO_2(anatase) similarly method as Ni_2P/TiO_2-2.0P. Only Ni_2P species were detected. This emphasizes that the excess phosphorous as compared to Ni is required to synthesize the Ni_2P despite the different in surface area and acidity/basicity of the support.

Ni_2P species in Ni_2P/TiO_2-2.0P can selectively catalyze the ethane steam cracking at 650°C to ethylene (>99.0%) with the ethane conversion rate of 65.2 $mmol_{ethane}\cdot g_{Ni}^{-1}\cdot h^{-1}$. While metallic Ni in Ni/TiO_2 would provide mainly syn gas products (80% selectivity). The presence of $Ni_{12}P_5$ as a mixed nickel phosphide species in Ni_xP_y/TiO_2-0.5P leads to a lower in both ethane conversion rate (43.5 $mmol_{ethane}\cdot g_{Ni}^{-1}\cdot h^{-1}$) and ethylene selectivity (72.2%). Both surface area and metal strong interaction between Ni_2P and TiO_2 play an important role in the ethane steam cracking reaction as proved by Ni_2P/TiO_2(anatase)-2.0P, Ni_2P/SiO_2-2.0P, and Ni_2P/TiO_2(Phy). Even though Ni_2P/TiO_2-2.0P provided a high ethylene selectivity. The changes in Ni_2P species to

metallic Ni was observed after time on steam of 11 h. The transformation of Ni_2P to metallic Ni was also evidenced in the *in-situ* XANES upon reduction under atmospheric H_2 pressure at 650°C.

5.2 Suggestion

5.2.1 To improve ethylene productivity, the various of steam to ethane ratio should be investigated.

5.2.2 The reaction temperature of ethane steam cracking over Ni_2P catalysts should be further studied.

5.2.3 The interaction between Ni_2P and reducible supports play an importance role to enhance both of ethane conversion rate and ethylene selectivity. For further study, the reducible supports such as ZrO_2 and CeO_2 should be evaluated. On the other hand, the Ni_2P synthesis method (such as sol-gel method) should also be considered.

REFERENCE

[1] CPMA. 2021. **Ethylene.** [Online]. Available : http://cpmaindia.com/ethylene_about.php.

[2] T.O.G. Journal. 2010. **OGJ FOCUS:Global ethylene production.** [Online]. Available : https://www.ogj.com/articles/print/volume-108/issue-27/technology/ogj-focus-global-ethylene.html.

[3] T. Ren, M. Patel, K. Blok. 2006. "Olefins from conventional and heavy feedstocks: Energy use in steam cracking and alternative processes." *Energy* 31(4): 425-451.

[4] M. Yang, X. Tian, F. You. 2018. "Manufacturing ethylene from wet shale gas and biomass: comparative technoeconomic analysis and environmental life cycle assessment." *Industrial & Engineering Chemistry Research* 57(17): 5980-5998.

[5] O.A. Bariås, A. Holmen, E.A. Blekkan. 1996. "Propane dehydrogenation over supported Pt and Pt–Sn catalysts: catalyst preparation, characterization, and activity measurements." *J. Catal.* 158(1): 1-12.

[6] T. Zhang, M.D. Amiridis. 1998. "Hydrogen production via the direct cracking of methane over silica-supported nickel catalysts." *Appl. Catal., A* 167(2): 161-172.

[7] A. Jukić. 2013. **Production of Olefins – Steam Cracking of Hydrocarbons.** [Online]. Available : https://www.fkit.unizg.hr/_download/repository/PRPP_2013_Steam _cracking_Olefins.pdf.

[8] J. Sinfelt. 1970. "Catalytic hydrogenolysis over supported metals." *Catalysis Reviews* 3(1): 175-205.

[9] J. Sinfelt, Specificity in catalytic hydrogenolysis by metals, in: Advances in catalysis, Elsevier, 1973, pp. 91-119.

[10] J.H. Sinfelt, D.J. Yates. 1967. "Catalytic hydrogenolysis of ethane over the noble metals of Group VIII." *J. Catal.* 8(1): 82-90.

[11] M. Matsukata, T. Matsushita, K. Ueyama. 1996. "A novel hydrogen/syngas production process: Catalytic activity and stability of $NiSiO_2$." *Chem. Eng. Sci.* 51(11): 2769-2774.

[12] K. Otsuka, S. Kobayashi, S. Takenaka. 2000. "Decomposition and regeneration of methane in the absence and the presence of a hydrogen-absorbing alloy $CaNi_5$." *Appl. Catal., A* 190(1-2): 261-268.

[13] K. Otsuka, T. Seino, S. Kobayashi, S. Takenaka. 1999. "Production of hydrogen through decomposition of methane with Ni-supported catalysts." *Chem. Lett.* 28(11): 1179-1180.

[14] B. Monnerat, L. Kiwi-Minsker, A. Renken. 2001. "Hydrogen production by catalytic cracking of methane over nickel gauze under periodic reactor operation." *Chem. Eng. Sci.* 56(2): 633-639.

[15] S.Y. Chin, Y.-H. Chin, M.D. Amiridis. 2006. "Hydrogen production via the catalytic cracking of ethane over Ni/SiO_2 catalysts." *Appl. Catal., A* 300(1): 8-13.

[16] R. Aiello, J.E. Fiscus, H.-C. Zur Loye, M.D. Amiridis. 2000. "Hydrogen production via the direct cracking of methane over Ni/SiO2: catalyst deactivation and regeneration." *Appl. Catal., A* 192(2): 227-234.

[17] S.A. Sarris, N. Olahova, K. Verbeken, M.-F.o. Reyniers, G.B. Marin, K.M. Van Geem. 2017. "Optimization of the in situ pretreatment of high temperature Ni–Cr alloys for ethane steam cracking." *Industrial & Engineering Chemistry Research* 56(6): 1424-1438.

[18] L. Yang, X. Li, A. Wang, R. Prins, Y. Wang, Y. Chen, X. Duan. 2014. "Hydrodesulfurization of 4, 6-dimethyldibenzothiophene and its hydrogenated intermediates over bulk Ni_2P." *J. Catal.* 317: 144-152.

[19] P.S. Krishnan, R. Ramya, S. Umasankar, K. Shanthi. 2017. "Promotional effect of Ni_2P on mixed and separated phase MoS_2/Al-SBA-15 (10) catalyst for hydrodenitro- genation of ortho-Propylaniline." *Microporous Mesoporous Mater.* 242: 208-220.

[20] D. Li, P. Bui, H. Zhao, S. Oyama, T. Dou, Z. Shen. 2012. "Rake mechanism for the deoxygenation of ethanol over a supported Ni_2P/SiO_2 catalyst." *J. Catal.* 290: 1-12.

[21] L. Nan, C. Yang, L. Jin, G. Wei, Z.-w. ZHAO. 2016. "Preparation of Ni_2P/Zr-MCM-41 catalyst and its performance in the hydrodeoxygenation of Jatropha curcas oil." *Journal of Fuel Chemistry and Technology* 44(1): 76-83.

[22] T.I. Korányi. 2003. "Phosphorus promotion of Ni (Co)-containing Mo-free catalysts in thiophene hydrodesulfurization." *Appl. Catal., A* 239(1-2): 253-267.

[23] P.A. Clark, S.T. Oyama. 2003. "Alumina-supported molybdenum phosphide hydroprocessing catalysts." *J. Catal.* 218(1): 78-87.

[24] P. Clark, X. Wang, S.T. Oyama. 2002. "Characterization of silica-supported molybdenum and tungsten phosphide hydroprocessing catalysts by ^{31}P nuclear magnetic resonance spectroscopy." *J. Catal.* 207(2): 256-265.

[25] S. Oyama, X. Wang, Y.-K. Lee, K. Bando, F. Requejo. 2002. "Effect of phosphorus content in nickel phosphide catalysts studied by XAFS and other techniques." *J. Catal.* 210(1): 207-217.

[26] Y.-S. Kim, G.-N. Yun, Y.-K. Lee. 2014. "Novel Ni_2P/zeolite catalysts for naphthalene hydrocracking to BTX." *Catal. Commun.* 45: 133-138.

[27] S.J. Sawhill, D.C. Phillips, M.E. Bussell. 2003. "Thiophene hydrodesulfurization over supported nickel phosphide catalysts." *J. Catal.* 215(2): 208-219.

[28] R. Wang, K.J. Smith. 2009. "Hydrodesulfurization of 4, 6-dimethyldibenzothiophene over high surface area metal phosphides." *Appl. Catal., A* 361(1-2): 18-25.

[29] X. Li, Y. Zhang, A. Wang, Y. Wang, Y. Hu. 2010. "Influence of TiO2 and CeO2 on the hydrogenation activity of bulk Ni_2P." *Catal. Commun.* 11(14): 1129-1132.

[30] K. Wang, B. Yang, Y. Liu, C. Yi. 2009. "Preparation of $Ni_2P/TiO_2–Al_2O_3$ and the catalytic performance for hydrodesulfurization of 3-methylthiophene." *Energy Fuels* 23(9): 4209-4214.

[31] N.W. Encyclopedia. 2017. **Ethylene.** [Online]. Available : https://www.newworldencyclopedia.org/entry/Ethylene.

[32] Wikipedia. 2022. **Linear low-density polyethylene.** [Online]. Available : https://en.wikipedia.org/wiki/Linear_low-density_polyethylene.

[33] Wikipedia. 2022. **High-density polyethylene.** [Online]. Available : https://en.wikipedia.org/wiki/High-density_polyethylene.

[34] Wikipedia. 2022. **Ethylene oxide.** [Online]. Available : https://en.wikipedia.org/wiki/Ethylene_oxide.

[35] Wikipedia. 2022. **Ethyl acetate.** [Online]. Available : https://en.wikipedia.org/wiki/Ethyl_acetate.

[36] Wikipedia. 2022. **Ethane.** [Online].
Available : https://en.wikipedia.org/wiki/Ethane.

[37] C. PRODUCTIONS. 2020. **NATURAL GAS COMPOSITION.** [Online].
Available : https://www.croftsystems.net/oil-gas-blog/natural-gas-composition.

[38] V. Köster. 2013. **What is Shale Gas? How Does Fracking Work?** [Online].
Available : https://www.chemistryviews.org/details/education/1316813/What_is_ Shale_Gas_How_Does_Fracking_Work/.

[39] B. Bowman. 2016. **CMR FlexPO Shale Gas 2012.** [Online].
Available : http://www.adi-cmr.com/wp-content/uploads/2016/03/CMR-FlexPO-Shale-Gas-2012-Bob-Bowman.pdf.

[40] A. Ausavasukhi, T. Sooknoi. 2014. "Tunable activity of [Ga] HZSM-5 with H_2 treatment: Ethane dehydrogenation." *Catal. Commun.* 45: 63-68.

[41] Z. Wu, E.C. Wegener, H.-T. Tseng, J.R. Gallagher, J.W. Harris, R.E. Diaz, Y. Ren, F.H. Ribeiro, J.T. Miller. 2016. "Pd–In intermetallic alloy nanoparticles: highly selective ethane dehydrogenation catalysts." *Catal. Sci. Technol.* 6(18): 6965-6976.

[42] B. Fu, J. Lu, P.C. Stair, G. Xiao, M.C. Kung, H.H. Kung. 2013. "Oxidative dehydrogenation of ethane over alumina-supported Pd catalysts. Effect of alumina overlayer." *J. Catal.* 297: 289-295.

[43] R. Curley. 2012. **cracking chemical process.** [Online].
Available : https://www.britannica.com/technology/cracking-chemical-process.

[44] Wikipedia. 2022. **Cracking (chemistry).** [Online].
Available : https://en.wikipedia.org/wiki/Cracking_(chemistry).

[45] Wikipedia. 2022. **Thermal cracking.** [Online]. Available : https://en.wikipedia.org/wiki/Cracking_(chemistry)#Thermal_cracking.

[46] W. Appleby, J. Gibson, G. Good. 1962. "Coke formation in catalytic cracking." *Industrial & Engineering Chemistry Process Design and Development* 1(2): 102-110.

[47] G. Taralas. 1996. "Catalytic steam cracking of n-heptane with special reference to the effect of calcined dolomite." *Industrial & engineering chemistry research* 35(7): 2121-2126.

[48] S.T. Oyama, X. Wang, Y.-K. Lee, W.-J. Chun. 2004. "Active phase of Ni_2P/SiO_2 in hydroprocessing reactions." *J. Catal.* 221(2): 263-273.

[49] Y. Shu, Y.-K. Lee, S.T. Oyama. 2005. "Structure-sensitivity of hydrodesulfurization of 4, 6-dimethyldibenzothiophene over silica-supported nickel phosphide catalysts." *J. Catal.* 236(1): 112-121.

[50] Wikipedia. 2022. **Silicon dioxide.** [Online]. Available : https://en.wikipedia.org/wiki/Silicon_dioxide.

[51] L.-B. Xiong, J.-L. Li, B. Yang, Y. Yu. 2012. "Ti3+ in the Surface of Titanium Dioxide: Generation, Properties and Photocatalytic Application." *Journal of Nanomaterials* 2012.

[52] S. Wendt, R. Schaub, J. Matthiesen, E.K. Vestergaard, E. Wahlström, M.D. Rasmussen, P. Thostrup, L. Molina, E. Lægsgaard, I. Stensgaard. 2005. "Oxygen vacancies on TiO2 (1 1 0) and their interaction with H_2O and O_2: A combined high-resolution STM and DFT study." *Surf. Sci.* 598(1-3): 226-245.

[53] Z. Zhang, J. Long, X. Xie, H. Zhuang, Y. Zhou, H. Lin, R. Yuan, W. Dai, Z. Ding, X. Wang. 2012. "Controlling the synergistic effect of oxygen vacancies and N dopants to enhance photocatalytic activity of N-doped TiO_2 by H_2 reduction." *Appl. Catal., A* 425: 117-124.

[54] M.W. van Goethem, S. Barendregt, J. Grievink, P.J. Verheijen, M. Dente, E. Ranzi. 2013. "A kinetic modelling study of ethane cracking for optimal ethylene yield." *Chem. Eng. Res. Des.* 91(6): 1106-1110.

[55] R. Dutta, M. McCaffrey, M. Gray, Effect of Steam on Coking Chemistry of Athabasca Bitumen, in: Abstracts of Papers Of The American Chemical Society, 1999, pp. 218.

[56] H. Chen, J. Tan, Y. Zhu, Y. Li. 2016. "An effective and stable Ni_2P/TiO_2 catalyst for the hydrogenation of dimethyl oxalate to methyl glycolate." *Catal. Commun.* 73: 46-49.

[57] H. Song, M. Dai, H. Song, X. Wan, X. Xu, C. Zhang, H. Wang. 2014. "Synthesis of a Ni_2P catalyst supported on anatase–TiO_2 whiskers with high hydrodesulfurization activity, based on triphenylphosphine." *Catal. Commun.* 43: 151-154.

[58] L.-h. LIU, S.-q. LIU, H.-l. YIN, Y.-q. LIU, C.-g. LIU. 2015. "Hydrogen spillover effect between Ni_2P and MoS_2 catalysts in hydrodesulfurization of dibenzothiophene." *Journal of Fuel Chemistry and Technology* 43(6): 708-713.

[59] Z.-j. Wang, P. Wu, L. Lan, K. Liu, Y. Hu, S. Ji. 2015. "Preparation, characterization and hydrodesulfurization performances of Co-Ni_2P/SBA-15 catalysts." *Journal of Energy Chemistry* 24(2): 185-192.

[60] X. Lan, E.J. Hensen, T. Weber. 2017. "Silica-supported Ni_2P: Effect of preparation conditions on structure and catalytic performance in thiophene hydrodesulfuriza- tion (HDS)." *Catal. Today* 292: 121-132.

[61] Q. Guan, X. Cheng, R. Li, W. Li. 2013. "A feasible approach to the synthesis of nickel phosphide for hydrodesulfurization." *J. Catal.* 299: 1-9.

[62] Q. Sheng, X. Li, R. Prins, C. Liu, Q. Hao, S. Chen. 2021. "Understanding the Reduction of Transition-Metal Phosphates to Transition-Metal Phosphides by Combining Temperature-Programmed Reduction and Infrared Spectroscopy." *Angewandte Chemie* 133(20): 11280-11283.

[63] S. Hua, G. Jing, N. JIANG, L. Feng, D. Min, J.-j. ZHANG, D.-z. YU. 2016. "Effect of P/Ni molar ratio on the structure and hydrodesulfurization performance of nickel phosphide catalyst prepared by the solvothermal method." *Journal of Fuel Chemistry and Technology* 44(5): 557-563.

[64] C. Stinner, Z. Tang, M. Haouas, T. Weber, R. Prins. 2002. "Preparation and ^{31}P NMR characterization of nickel phosphides on silica." *Journal of Catalysis* 208(2): 456-466.

[65] Z. Xu, S. Wang, C. Ma, K. Luo, F. Fang. 2019. "Effect of Nickel Doping on Phase Transformation of TiO_2 Nanotube Arrays." *physica status solidi (a)* 216(6): 1800836.

[66] J. Espinós, A. González-Elipe, G. Munuera. 1993. "Diffusion of nickel and surface reconstruction in Ni/TiO_2 catalysts promoted by H_2 and O_2 treatments." *Solid state ionics* 63: 748-754.

[67] N.O. Gopal, H.-H. Lo, T.-F. Ke, C.-H. Lee, C.-C. Chou, J.-D. Wu, S.-C. Sheu, S.-C. Ke. 2012. "Visible light active phosphorus-doped TiO_2 nanoparticles: an EPR evidence for the enhanced charge separation." *The Journal of Physical Chemistry C* 116(30): 16191-16197.

[68] J.A. Rodriguez, J.-Y. Kim, J.C. Hanson, S.J. Sawhill, M.E. Bussell. 2003. "Physical and chemical properties of MoP, Ni_2P, and MoNiP hydrodesulfurization catalysts: time-resolved X-ray diffraction, density functional, and hydrodesulfurization activity studies." *J. Phys. Chem. B* 107(26): 6276-6285.

[69] S. Zhang, J. Wang, X. Wang. 2008. "Effect of calcination temperature on structure and performance of Ni/TiO_2-SiO_2 catalyst for CO_2 reforming of methane." *Journal of Natural Gas Chemistry* 17(2): 179-183.

[70] R. Wang, K.J. Smith. 2010. "The effect of preparation conditions on the properties of high-surface area Ni_2P catalysts." *Applied Catalysis A: General* 380(1-2): 149-164.

[71] X. Wang, Y. Liu, K. Liu, J. Zhang, J. Wei. 2020. "Phosphorus-tuned nickel as high coke-resistant catalyst with high reforming activity." *International Journal of Hydrogen Energy* 45(53): 28325-28336.

[72] T.I. Korányi, Z. Vít, D.G. Poduval, R. Ryoo, H.S. Kim, E.J. Hensen. 2008. "SBA-15-supported nickel phosphide hydrotreating catalysts." *Journal of Catalysis* 253(1): 119-131.

[73] X. Wang, P. Clark, S.T. Oyama. 2002. "Synthesis, characterization, and hydrotreating activity of several iron group transition metal phosphides." *Journal of Catalysis* 208(2): 321-331.

[74] T. Uchikoshi, Y. Sakka, S. Ohno, H. Okuyama, K. Yoshihara. 1993. "Adsorption of hydrogen on Ni and Ni□ TiO_2 composite ultrafine particles." *Surface science* 287: 1082-1086.

[75] V.M. Shinde, G. Madras. 2014. "CO methanation toward the production of synthetic natural gas over highly active Ni/TiO_2 catalyst." *AIChE Journal* 60(3): 1027-1035.

[76] U. Pittermann, S. Ripper. 1986. "Crystallization Behaviour of Thin NiP Alloy Films Prepared by Electroless or Galvanic Deposition." *physica status solidi (a)* 93(1): 131-142.

[77] S.-K. Wu, P.-C. Lai, Y.-C. Lin, H.-P. Wan, H.-T. Lee, Y.-H. Chang. 2013. "Atmospheric hydrodeoxygenation of guaiacol over alumina-, zirconia-, and silica-supported nickel phosphide catalysts." *ACS Sustainable Chemistry & Engineering* 1(3): 349-358.

[78] T.I. Korányi, E.J. Hensen. 2017. "Preparative aspects of supported Ni_2P catalysts for reductive upgrading of technical lignin to aromatics." *Catalysis Letters* 147(7): 1722-1731.

[79] L. Feitosa, G. Berhault, D. Laurenti, V.T. da Silva, Guaiacol hydrodeoxigenation over carbon supported nickel phosphide (Ni_2P/C)–the effect of carbon support on synthesis and catalytic activity, in: Europacat 2017, 2017.

[80] S. Gutiérrez-Rubio, A. Berenguer, J. Přech, M. Opanasenko, C. Ochoa-Hernández, P. Pizarro, J. Čejka, D.P. Serrano, J.M. Coronado, I. Moreno. 2020. "Guaiacol hydrodeoxygenation over Ni_2P supported on 2D-zeolites." *Catalysis Today* 345: 48-58.

[81] J. Ko, J.A. Muhlenkamp, Y. Bonita, N.J. LiBretto, J.T. Miller, J.C. Hicks, W.F. Schneider. 2020. "Experimental and Computational Investigation of the Role of P in Moderating Ethane Dehydrogenation Performance over Ni-Based Catalysts." *Industrial & Engineering Chemistry Research* 59(28): 12666-12676.

[82] R.T. Vang, K. Honkala, S. Dahl, E.K. Vestergaard, J. Schnadt, E. Lægsgaard, B.S. Clausen, J.K. Nørskov, F. Besenbacher. 2005. "Controlling the catalytic bond-breaking selectivity of Ni surfaces by step blocking." *Nature materials* 4(2): 160-162.

[83] L. Zhang, X. Wang, B. Tan, U.S. Ozkan. 2009. "Effect of preparation method on structural characteristics and propane steam reforming performance of Ni–Al_2O_3 catalysts." *J. Mol. Catal. A: Chem.* 297(1): 26-34.

[84] Q. Zhu, H. Zhang, S. Zhang, G. Wang, X. Zhu, C. Li. 2019. "Dehydrogenation of isobutane over a Ni–P/SiO_2 catalyst: Effect of P addition." *Industrial & Engineering Chemistry Research* 58(19): 7834-7843.

[85] J.Z. Chen, J. Gao, P.R. Probus, W. Liu, X. Wu, E.C. Wegener, A.J. Kropf, D. Zemlyanov, G. Zhang, X. Yang. 2020. "The effect of strong metal–support interaction (SMSI) on Pt–Ti/SiO_2 and Pt–Nb/SiO_2 catalysts for propane dehydrogenation." *Catal. Sci. Technol.* 10(17): 5973-5982.

APPENDICES

APPENDIX A

EXAMPELS OF CALCULATION

Contact time, *W/F*

Calculation of catalytic parameter W/F:

$$W/F = \frac{\text{Weight of catalyst (g)}}{\text{Molar feed rate (mol/h)}}$$

In the reaction using feed rate 1,476 mL/h of ethane as the feed and using 0.44 gram of catalyst, the *W/F* is calculated as follows:

$$W/F = \frac{[0.44\ g_{catalyst}][30.07\ (g_{Ethane}/mol_{Ethane})]}{[1{,}474.95\ (mL_{Ethane}/h)][0.001264\ (g_{Ethane}/mL_{Ethane})]}$$

$$= 7.3\ g.h/mol$$

In similar manner, *W/F* of catalyst with different mass and different feed rate can be calculated.

Calculation of %yield of products from gas chromatography

Table A1 The summation of the peak area for products

Product	Peak area
Methane	3,519
Ethane (feed)	9,782,957
Ethylene	332,938
Total	10,119,414

* Information of ethane over Ni_2P/TiO_2-2.0P; *W/F* = 7.3 $g_{catalyst}{\cdot}h{\cdot}mol_{Ethane}^{-1}$, atmospheric pressure. The values shown were taken at 210 minutes time on stream.

.

In normalization method, the areas of all eluted peaks were computed, taking into account the differences in the detector response to different compound types.

The concentration of the analyzed species was found from the ratio of its area to the total area of all peaks.

The calculation of the percent yield of each component in the sample follows:

$$\%\text{yield of product A} = \frac{\text{Peak area of A} \times 100}{\text{Total area}}$$

For example,

$$\%\text{yield of Ethylene} = \frac{332938 \times 100}{10119414}$$

$$= 3.29\%$$

The percent yield of each product obtained from above calculation is shown below.

Table A2 Yield of products derived by normalization method.

Products	**%Yield**
Methane	0.03
Ethane (feed)	96.68
Ethylene	3.29
Total	100

Conversion

%Conversion can be calculated from the following equation:

$$\%\text{Conversion} = \frac{\text{Area total - Area feed}}{\text{Area total}} \times 100$$

For example,

$$\%\text{Conversion} = \frac{10119414 - 9782957}{10119414} \times 100$$

$$= 3.32\%$$

Selectivity

%Selectivity can be obtained from the following equation:

$$\%\text{Selectivity in each product} = \frac{\%\text{Yield of each product} \times 100}{\%\text{Conversion}}$$

For example,

$$\%\text{Selectivity of Butanol} = \frac{3.29 \times 100}{3.32}$$

$$= 99.10\%$$

Ethane conversion rate

Ethane conversion rate can be obtained from the following equation:

$$\text{Ethane conversion rate} = \frac{\text{Molar feed rate (mol/h)} \times \%\text{Conversion}}{\text{Weight of catalyst (g)} \times \%\text{weight of Ni}}$$

For example,

$$\text{Ethane conversion rate} = \frac{[1{,}474.95\ (\text{mL/h})][0.001264\ (g_{Ethane}/\text{mL})][3.32\%]}{[0.44\ g_{catalyst}][30.07\ (g_{Ethane}/\text{mol})][7\ \text{wt.\%}]}$$

$$= 65.2\ \text{mmol}_{Ethane} \cdot g_{Ni}^{-1} \cdot h^{-1}$$

The percent theoretical composition of each catalyst obtained from above calculation is shown in **Table 4.3**.

APPENDIX B

GAS CHROMATOGRAM

Prior to analysis, the identification of each product was performed by GC-MS (gas chromatography with mass spectrometer detector). Then, the quantitative analysis of each product was carried out by GC-FID (gas chromatography with flame ionization detector) with the condition expressed in **Table B1**.

Table B1 The GC condition for quantitative analysis

Column	HP-Plot (50m, 0.53mm ID, 6μm Rt-Alumina^{TM} PLOT)
Temperature program	80 °C (hold 4 min) to 150 °C, rate 10 °C/min (hold 9 min)
Split ratio	50:1
GC carrier gas	N_2 gas
Injector temperature	250 °C
Detector temperature	FID (280 °C)
Linear velocity	22.1 cm/sec

The products formed eluted at the following retention time listed in **Table B2.**

Table B2 Retention time of products and feed

Feed or Products	**Retention time (min)**
Methane	2.6
Ethane	2.9
Ethylene	3.5

APPENDIX C

CATALYTIC ACTIVITY DATA

In all cases, the following reaction condition was applied: temperature: 650 °C; activation in H_2 at 650 °C for 120 min; pressure: 1 atm; contact time: 7.3 $g_{catalyst}$·h·mol_{Ethane}^{-1}.

Table C1 Ethane conversion and yield of products over Ni_2P/TiO_2-2.0P

Time on stream (min)	**30**	**75**	**120**	**165**	**210**
Conversion (%)	1.41	2.16	2.02	2.50	3.32
Yield of product (%)					
Methane	0.00	0.01	0.01	0.02	0.03
Ethylene	1.41	2.15	2.01	2.48	3.29
Syn gas	0.00	0.00	0.00	0.00	0.00
Coke	0.00	0.00	0.00	0.00	0.00

Reaction condition: T_{react} = 650 °C, F_{Ethane} = 24.6 mL/min (99.95%), W/F = 7.3 $g_{catalyst}$·h·mol_{Ethane}^{-1}, atmospheric pressure. The values shown were taken at 210 minutes time on stream.

Table C2 Ethane conversion and yield of products over Ni/TiO_2

Time on stream (min)	**30**	**75**	**120**	**165**	**210**
Conversion (%)	100	100	100	100	100
Yield of product (%)					
Methane	8.89	8.89	8.89	8.89	8.89
Ethylene	0.00	0.00	0.00	0.00	0.00
Syn gas	80.04	80.04	80.04	80.04	80.04
Coke	11.07	11.07	11.07	11.07	11.07

Reaction condition: T_{react} = 650 °C, F_{Ethane} = 24.6 mL/min (99.95%), W/F = 7.3 $g_{catalyst}$·h·mol_{Ethane}^{-1}, atmospheric pressure. The values shown were taken at 210 minutes time on stream.

Table C3 Ethane conversion and yield of products over Ni_xP_y/TiO_2-0.5P

Time on stream (min)	**30**	**75**	**120**	**165**	**210**
Conversion (%)	3.58	1.91	1.76	1.72	1.78
Yield of product (%)					
Methane	0.04	0.03	0.17	0.03	0.03
Ethylene	3.54	1.88	1.58	1.68	1.76
Syn gas	0.00	0.00	0.00	0.00	0.00
Coke	0.02	0.01	0.01	0.01	0.01

Reaction condition: T_{react} = 650 °C, F_{Ethane} = 24.6 mL/min (99.95%), W/F = 7.3 $g_{catalyst}{\cdot}h{\cdot}mol_{Ethane}^{-1}$, atmospheric pressure. The values shown were taken at 210 minutes time on stream.

Table C4 Ethane conversion and yield of products over Ni_2P/TiO_2(anatase)-2.0P

Time on stream (min)	**30**	**75**	**120**	**165**	**210**
Conversion (%)	0.77	1.12	1.15	1.27	1.24
Yield of product (%)					
Methane	0.00	0.00	0.00	0.00	0.00
Ethylene	0.77	1.12	1.15	1.27	1.24
Syn gas	0.00	0.00	0.00	0.00	0.00
Coke	0.00	0.00	0.00	0.00	0.00

Reaction condition: T_{react} = 650 °C, F_{Ethane} = 24.6 mL/min (99.95%), W/F = 7.3 $g_{catalyst}{\cdot}h{\cdot}mol_{Ethane}^{-1}$, atmospheric pressure. The values shown were taken at 210 minutes time on stream.

Table C5 Ethane conversion and yield of products over Ni_2P/SiO_2-2.0P

Time on stream (min)	**30**	**75**	**120**	**165**	**210**
Conversion (%)	1.71	1.34	1.24	1.24	1.21
Yield of product (%)					
Methane	0.00	0.00	0.00	0.00	0.00
Ethylene	1.71	1.34	1.24	1.24	1.21
Syn gas	0.00	0.00	0.00	0.00	0.00
Coke	0.00	0.00	0.00	0.00	0.00

Reaction condition: T_{react} = 650 ℃, F_{Ethane} = 24.6 mL/min (99.95%), W/F = 7.3 $g_{catalyst}{\cdot}h{\cdot}mol_{Ethane}^{-1}$, atmospheric pressure. The values shown were taken at 210 minutes time on stream.

Table C6 Ethane conversion and yield of products over Ni_2P/SiO_2-2.0P

Time on stream (min)	**30**	**75**	**120**	**165**	**210**
Conversion (%)	0.90	0.78	0.81	0.90	1.01
Yield of product (%)					
Methane	0.00	0.00	0.00	0.00	0.00
Ethylene	0.90	0.78	0.81	0.90	1.01
Syn gas	0.00	0.00	0.00	0.00	0.00
Coke	0.00	0.00	0.00	0.00	0.00

Reaction condition: T_{react} = 650 ℃, F_{Ethane} = 24.6 mL/min (99.95%), W/F = 7.3 $g_{catalyst}{\cdot}h{\cdot}mol_{Ethane}^{-1}$, atmospheric pressure. The values shown were taken at 210 minutes time on stream.

Table C7 Ethane conversion and yield of products over Ni_2P/TiO_2-2.0P at *W/F* = 3.6 $g_{catalyst}{\cdot}h{\cdot}mol_{Ethane}^{-1}$

Time on stream (min)	**30**	**75**	**120**	**165**	**210**
Conversion (%)	1.41	1.41	1.75	2.02	2.31
Yield of product (%)					
Methane	0.00	0.00	0.00	0.01	0.02
Ethylene	1.41	1.41	1.75	2.01	2.29
Syn gas	0.00	0.00	0.00	0.00	0.00
Coke	0.00	0.00	0.00	0.00	0.00

Reaction condition: T_{react} *= 650 °C,* F_{Ethane} *= 24.6 mL/min (99.95%), atmospheric pressure. The values shown were taken at 210 minutes time on stream.*

Table C8 Ethane conversion and yield of products over Ni_2P/TiO_2-2.0P at *W/F* = 5.5 $g_{catalyst}{\cdot}h{\cdot}mol_{Ethane}^{-1}$

Time on stream (min)	**30**	**75**	**120**	**165**	**210**
Conversion (%)	1.13	1.82	2.29	2.83	3.48
Yield of product (%)					
Methane	0.00	0.00	0.01	0.02	0.04
Ethylene	1.13	1.82	2.28	2.81	3.44
Syn gas	0.00	0.00	0.00	0.00	0.00
Coke	0.00	0.00	0.00	0.00	0.00

Reaction condition: T_{react} *= 650 °C,* F_{Ethane} *= 24.6 mL/min (99.95%), atmospheric pressure. The values shown were taken at 210 minutes time on stream.*

Ethane conversion and yield of products over Ni_2P/TiO_2-2.0P at *W/F* = 7.3 $g_{catalyst}{\cdot}h{\cdot}mol_{Ethane}^{-1}$ has seen in **Table C1**

Table C9 Ethane conversion and yield of products over Ni_2P/TiO_2-2.0P at *W/F* = 9.1 $g_{catalyst} \cdot h \cdot mol_{Ethane}^{-1}$

Time on stream (min)	**30**	**75**	**120**	**165**	**210**
Conversion (%)	1.90	2.14	2.43	3.07	3.40
Yield of product (%)					
Methane	0.00	0.01	0.02	0.03	0.04
Ethylene	1.89	2.12	2.40	3.03	3.35
Syn gas	0.00	0.00	0.00	0.00	0.00
Coke	0.01	0.01	0.01	0.01	0.01

Reaction condition: T_{react} = 650 °C, F_{Ethane} = 24.6 mL/min (99.95%), atmospheric pressure. The values shown were taken at 210 minutes time on stream.

Table C10 Ethane conversion and yield of products over Ni_2P/TiO_2-2.0P in 11 h TOS

Time on stream (min)	**30**	**75**	**120**	**165**	**210**	**255**	**300**	**345**	**390**	**435**	**525**	**570**	**615**	**660**
Conversion (%)	1.41	2.16	2.02	2.50	3.32	2.87	3.83	2.95	2.42	2.01	2.25	1.95	2.18	2.16
Yield of product (%)														
Methane	0.00	0.01	0.01	0.02	0.03	0.02	0.03	0.03	0.03	0.03	0.09	0.12	0.10	0.11
Ethylene	1.41	2.15	2.01	2.48	3.29	2.80	3.74	2.87	2.35	1.95	2.16	1.83	2.08	2.05
Syn gas	0.00	0.00	0.00	0.00	0.00	0.00	0.00	0.00	0.00	0.00	0.00	0.00	0.00	0.00
Coke	0.00	0.00	0.00	0.00	0.00	0.05	0.06	0.05	0.04	0.03	0.00	0.00	0.00	0.00

Reaction condition: T_{react} *= 650 °C,* F_{Ethane} *= 24.6 mL/min (99.95%), W/F = 7.3* $g_{catalyst} \cdot h \cdot mol_{Ethane}^{-1}$*, atmospheric pressure. The values shown were taken at 660 minutes time on stream.*

Author Biography

Name	Miss Panisa Hongklai	
Date of Birth	27 January 1995	
Address		
Education	(2017) Bachelor of Science in Industrial chemistry	GPA 3.38
	King Mongkut's Institute of Technology Ladkrabang	
	(2022) Master of Science in Applied chemistry	GPA 3.62
	King Mongkut's Institute of Technology Ladkrabang	
Scholarship	The authors are grateful for financial support from the School of Science, KMITL.	

Academic Publication

1. P. Hongklai, P. Weerachawanasak, Y. Poo-arporn, K. Choojun, and T. Sooknoi, **"Ethylene Production from Catalytic Steam Cracking of Ethane over Nickel Phosphide Catalysts"** The 2020 Pure and Applied Chemistry International Conference (PACCON 2020).

PACCON 2020
Pure and Applied Chemistry International Conference
Chemistry for Catalyzing Sustainability and Prosperity

Ethylene production from catalytic steam cracking of ethane over nickel phosphide catalysts

Panisa Hongklai[1], Patcharaporn Weerachawanasak[1]*, Yingyot Poo-arporn[2], Kittisak Choojun[3]**, and Tawan Sooknoi[1,3]***

[1]*Department of Chemistry, Faculty of Science, King Mongkut's Institute of Technology Ladkrabang, Bangkok 10520, Thailand*

[2]*Synchrotron Light Research Institute (Public Organization), 111 University Avenue, Muang District, Nakhon Ratchasima 30000, Thailand*

[3]*Catalytic Chemistry Research Unit, Faculty of Science, King Mongkut's Institute of Technology Ladkrabang, Bangkok 10520, Thailand*

*E-mail:*patcharaporn.we@kmitl.ac.th,**kittisak.ch@kmitl.ac.th,***kstawan@gmail.com*

The use of ethane as an alternative feedstock for ethylene production has drawn much attention since the shale gas technology has developed. Catalytic steam cracking over supported metallic catalyst (Pd, Pt, Ni) can sufficiently provide high conversion at lower temperature (600-800˚C) compared with thermal steam cracking (>850˚C). However, they promote hydrogenolysis and coke formation causing low ethylene selectivity and stability. In this research, supported nickel phosphide (Ni_2P), possessing less metallic and water tolerant properties, was used as a catalyst for ethane steam cracking. 10%Ni_2P/TiO_2 catalyst was synthesized by co-impregnation method using $Ni(NO_3)_2{\cdot}6H_2O$ and $(NH_4)_2HPO_4$ ([Ni]/[P] ratio of 0.5), calcined and reduced at 500 and 650 ˚C, respectively. According to XRD, only crystalline of Ni_2P was observed in 10%Ni_2P/TiO_2. This corresponds to Ni:P amount determined by XRF. The conversion of ethane steam cracking in a fixed-bed reactor at 650˚C under atmospheric pressure is in the order of Thermal < TiO_2 (P25) < 10%Ni_2P/TiO_2 < 10%Ni/TiO_2 (1.9, 2.6, 6.4, 94.2%, respectively). Even though, 10%Ni/TiO_2 shows the highest activity, none of ethylene yield was observed. In sharp contrast, 57% ethylene selectivity was obtained from 10%Ni_2P/TiO_2, which was significantly higher than others. This emphasizes that Ni_2P is the active site for the C-H activation giving 100% ethylene selectivity.

1. Introduction

Ethylene is an important chemical feedstock for many chemical products.[1] The growth of global ethylene demand remains strong and the expectation of demand growth is in the range of 6.5 million metric tons per year.[2] For century, petroleum is the major source to produce ethylene, mainly steam cracking process. To meet the increasing demand of ethylene with the shortage of petroleum source, conversion of ethane to ethylene is an alternative promising strategy. This is due to the large supply of ethane from Shales and natural gases.[3] Hence, ethane could replace the obsolescent fossil-fuel-based feedstocks in the ethylene production.

The conventional process to convert ethane to ethylene is thermal cracking which requires high temperature with very low ethylene selectivity.[4] On the other hand, catalytic dehydrogenation of ethane using supported metals, such as Pt, Pd, and Ni, can improve the ethylene selectivity.[5] Chin *et al.* reported that the catalytic cracking of ethane over Ni/SiO_2 catalyst at 500˚C provides 95% conversion with 88% ethylene selectivity.[6] Once increase the temperature (600-650˚C), the ethylene selectivity was significantly dropped to 27%.[6] In addition, these catalysts show a fast deactivation due to coke formation even at relatively low temperature.

To reduce the coke deposition and prolong the catalyst life cycle, steam catalytic

CS19

cracking has been developed.[7] The introduction of steam as an inexpensive diluent of feed, can inhibit coke formation via competitive adsorption with coke precursor on the catalyst surfaces.[8] However, to operate under steam condition, most of active sites in noble metal catalysts cannot perform due to the oxidation reaction. As such, water tolerant property is the key factor of catalysts to operate in steam catalytic cracking.[9]

Nickel phosphide (Ni_2P) had been reported to operate and function in the extreme steam condition.[10] Matt *et al.* showed that supported metal phosphides on silica for the water-gas shift reaction.[11] Alvarez-Galvan *et al.* also reported that nickel phosphide catalysts were active towards hydrodeoxygenation reactions.[12] Chen *et al.* studied the effective and stability of bifunctional Ni_2P/TiO_2 catalyst for gas-phase hydrogenation of dimethyl oxalate to corresponding alcohols.[13] The catalyst showed a good stability upto at least 3600 h. The high stability of the nickel phosphide catalysts can be ascribed to i) semiconductor property of Ni_2P and ii) the strong interaction between Ni_2P and the support. Moreover, the small positive charge of Ni and the ensemble-effect of P in Ni_2P can also prevent the sintering of Ni_2P crystallites to enhance the stability at higher temperatures.[13]

With those regards, the catalytic steam cracking of ethane using supported nickel phosphide ($10\%Ni_2P/TiO_2$) as a catalyst was investigated as compared to typical steam cracking. In addition, the role nickel species in $10\%Ni_2P/TiO_2$ and $10\%Ni/TiO_2$ (supported nickel metallics) towards catalytic ethane steam cracking was studied. Both catalysts were characterized by XRF and BET. The nickel species was evaluated by XRD, H_2-TPR and *in-situ* XANES. All of the catalysts were tested using a continuous flow fixed-bed reactor at 650°C, 1 atm.

2. Materials and Methods

2.1 Materials

Ammonium dihydrogen phosphate ($(NH_4)_2HPO_4$, AR, QReC), Nickel(II) nitrate hexahydrate ($Ni(NO_3)_2{\cdot}6H_2O$, 99%, Carlo Erba), Titanium dioxide (TiO_2, P25, Degussa), Nitric acid (HNO_3, 69.50%, Carlo Erba) were purchased and used without further purification. Air (zero gas, 99.99%), H_2 (99.99%) and N_2 (99.99%) were ordered from UIG. Ethane (99.99%) was purchased from Linde.

2.2 Synthesis $10\%Ni/TiO_2$ and $10\%Ni_2P/TiO_2$

TiO_2 (P25) was dried at 70°C in an oven for 24 h prior use. To synthesis 10wt% of Ni/TiO_2 and Ni_2P/TiO_2, the calculated amount of TiO_2 was impregnated with the solution of nickel nitrate hexahydrate and the mixture of nickel nitrate hexahydrate and ammonium dihydrogen phosphate (Ni/P = 0.5) for $10\%Ni/TiO_2$ and $10\%Ni_2P/TiO_2$, respectively. Noted that a small amount of nitric acid was added to Ni and P solution to make it soluble. After that, the obtained samples were calcined at 500°C with a heating rate of 5°C/min for 6 h. Then, samples were reduced under H_2 (120 mL/min) at 650°C with a heating rate of 5°C/min for 2 h and passivated at room temperature in air for 15 min. This would result in the black solid of $10\%Ni/TiO_2$ and $10\%Ni_2P/TiO_2$ catalysts.

2.3 Characterization

The composition of the catalyst is studied by X-ray fluorescence (XRF) technique that can be done according to the following procedure 0.5 g of catalyst sample mixed with 4.5 g boric acid was compressed into alumina pan into the XRF sample holder in XRF instrument.

Gas adsorption analysis (Autosorb-1, Quantachrome) is used for determining surface area and pore size distribution of a catalyst. The sample of 100 mg was transferred to sample cell. This cell was attached to the outgassing station (300°C for 12 h). After the residual gas was removed by heating under vacuum, the cell was attached

to the sample station. Initially, a dewar of liquid nitrogen was placed to cool a sample cell. Nitrogen adsorbate pressure can be regulated by 1 torr transducer with 3 min equilibration time and 0 scaled tolerances.

The reducibility of the Ni and Ni_2P catalysts can be determined by a temperature-programmed reduction under H_2 gas (H_2-TPR). The experiments were carried out under 10%H_2 in Ar at a heating rate of 10˚C/min, from 50 to 900˚C. The effluent gases were analyzed using an online VICI thermal conductivity detector (TCD).

The oxidation state and species of nickel were evaluated using *in situ* X-ray near edge structure (*in situ* XANES) at BL2.2: TRXAS, Synchrotron Light Research Institute (SLRI), Thailand. An energy dispersive mono-chromator and position sensitive detector were employed to perform XANES measurement.[14] The Ni K-edge XANES was collected using the integration time of 2000 ms with an average of 10 scans. A 25 mg of calcined sample was weighted and pressed with a 5 mm diameter mold followed by placing into the sample holder. The *in-situ* experimental for reduction was operated by temperature-programming from 50-650˚C (5˚C/min) under a flow of 10%H_2 (30 mL/min) and held at 650˚C for 5 h. Then, XANES spectrum was collected. XANES spectra were processed over Athena software using Ni foil, NiO, and Ni_2P commercial as a standard.

2.4 Catalytic activity testing

The catalyst was packed into the middle of a quartz tube reactor covered with a quartz wool. The reactor was located at the center of a vertical tube furnace. Before activity testing, the nickel phosphide catalyst was be activated under H_2 (110 mL/min) at 650˚C (rate 10˚C/min) for 30 min. Then, steam and ethane were co-fed into the reactor by a syringe pumps and mass flow controller at the flow rate of 5.9 mL/h and 24.6 mL/min, respectively. The catalytic testing was conducted for the total time on stream (TOS) of 3.5 h. The products were detected by online-chromatography (GC).

3. Results & Discussion

3.1 Characterization

The surface area and elemental composition of 10%Ni/TiO_2 and 10%Ni_2P/TiO_2 is summarized in Table 1. The surface area of both catalysts (42 and 46 m^2/g for 10%Ni/TiO_2 and 10%Ni_2P/TiO_2, respectively) is lower than their parent (70 m^2/g). This could presumably due to the pore blocking of the incorporated Ni and/or P. The Ni and Ni_2P loadings of 10%Ni/TiO_2 and 10%Ni_2P/TiO_2 are 10wt% and 12.4wt%, respectively. For, 10%Ni_2P/TiO_2, Ni/P weight ratio (1.29) is relatively lower than the ideal Ni_2P species (3.76). This could attribute to the excess amount (4 equiv.) of the phosphorous precursor (phosphate, PO_4^{3-}) used during the synthesis to obtain the pure Ni_2P species, as reported by Oyama *et al.*[15] As such, some of phosphate and/or phosphorous could be remained in this sample after the reduction, resulting in the lower Ni/P weight ratio.

The XRD patterns of all both 10%Ni/TiO_2 and 10%Ni_2P/TiO_2 show the characteristic diffraction of P25 type of TiO_2. (Figure 1). The ratio of anatase to rutile of all samples are similar to their parent indicating that TiO_2(P25) remains unchanged during synthesis.

The 10%Ni/TiO_2 sample showed metallic Ni peaks at 2Θ = 45.5˚, 52.5˚ and 72.5˚. While, only Ni_2P diffraction peaks at 40.8˚, 44.5˚, 47.5˚ and 54.5˚ was observed in 10%Ni_2P/TiO_2.[16] This suggests that the only Ni_2P phase is obtained in this supported nickel phosphide catalyst.

Table 1. Physical properties and elemental content of each catalyst.

Entry	Sample	S_{BET} (m^2/g)	Content [a] (wt%)		
			Ni	P	Ni/P
1	TiO_2 (P25)	70	-	-	-
2	10%Ni/TiO_2	42	9.62	-	-
3	10%Ni_2P/TiO_2	46	6.97	5.39	1.29

[a] Determined by XRF

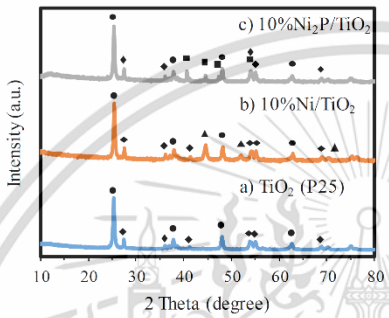

Figure 1. XRD pattern of TiO_2 (P25), 10%Ni/TiO_2 and 10%Ni_2P/TiO_2 catalysts. ((●) Anatase, (♦) Rutile, (▲) Ni, (■) Ni_2P).

In line with XRD, no nickel oxide (NiO) reduction peak was observed in temperature- programmed reduction (H_2-TPR) of Ni_2P/TiO_2 parent sample as shown in Figure 2. The typical reduction of Ni^{2+} to metallic Ni would show the reduction peak at 300-400°C, as detected in 10%Ni/TiO_2 parent sample (10%NiO/TiO_2, Figure 2a). In sharp contrast, Ni_2P/TiO_2 parent sample had a higher reduction (>450°C) which could attribute to the reduction of nickel pyrophosphate species ($Ni_2P_4O_{12}$/TiO_2) to form Ni_2P, as reported by Shamanaev *et al.*[17] Since Ni_2P is classified as a semiconductor, the formation of this species requires high reduction temperature, as observed in Figure 2.

The oxidation state of Ni species in both 10%Ni/TiO_2 and 10%Ni_2P/TiO_2 samples was studied using *in situ* X-ray near edge structure (*in situ* XANES), as shown in Figure 3. The Ni K-edge XANES spectra for the 10%Ni/TiO_2 is similar to that of Ni foil. In addition, the Ni K-edge energy of 10%Ni/TiO_2 is at 8,334 eV corresponding to metallic Ni. This result together with XRD and H_2-TPR strongly suggests the presence of metallic Ni species in 10%Ni/TiO_2 catalyst.

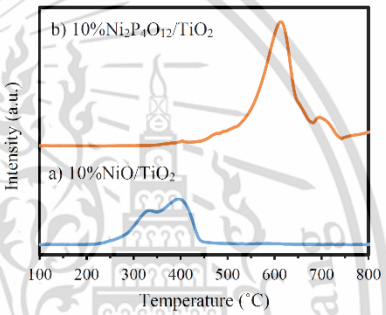

Figure 2. H_2-TPR of parent Ni and Ni_2P over TiO_2 samples.

The Ni K-edge energy of 10%Ni_2P/TiO_2 (8,340 eV) is higher than those of 10%Ni/TiO_2 (8,334 eV). Such higher in edge energy indicates that Ni species in 10%Ni_2P/TiO_2 possess a higher oxidation state. As the Ni species in Ni_2P having positive charge characteristics, this suggests the presence of Ni_2P species in 10%Ni_2P/TiO_2 catalysts. In supporting manner, the Ni K-edge energy of 10%Ni_2P/TiO_2 is similar to the commercial Ni_2P sample. This thus emphasizes the existence of Ni_2P in this supported nickel phosphide.

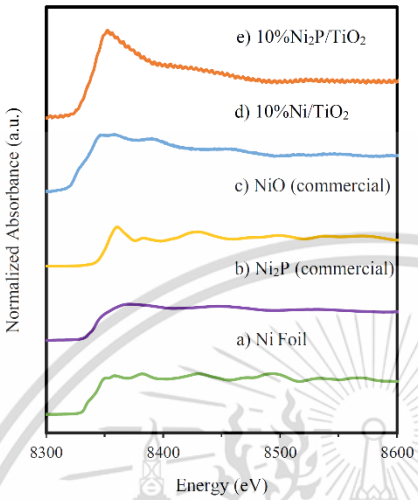

Figure 3. XANES spectra of Ni foil, Ni_2P, NiO, 10%Ni/TiO_2 and 10%Ni_2P/TiO_2.

3.2 Catalytic steam cracking of ethane to ethylene

The catalytic steam cracking of ethane was first evaluated using TiO_2 as a catalyst compared with thermal steam cracking in a fixed-bed reactor at 650°C under atmospheric pressure. According to Table 2, thermal steam cracking of ethane provides the lowest conversion (1.9%) with 40.2 and 59.8% selectivity of ethylene and C6+, respectively. The presence of TiO_2 (P25) enhances the conversion (2.5%), as compared thermal steam cracking (1.9%). While, the decrease in ethylene selectivity was observed, which could attribute to the formation of C6+ from ethylene conversion. This could indicate that the presence of TiO_2 promoted the ethylene coupling due to the presence of Lewis acid.[21]

The significant improvement in ethane conversion (96.1%) was observed once using 10%Ni/TiO_2 as a catalyst. However, >97% methane selectivity was obtained (Table 2, entry 3). This indicates that 10%Ni/TiO_2 promotes the hydrogenolysis yielding methane as a main product. It is worth noting that none of ethylene yield was detected in this experiment. The high activity of hydrogenolysis, could attribute to the metallic Ni representing in this catalyst. Hence, the C-C breaking of ethane is much more favorable than the C-H activation over metallic Ni catalysts.

In sharp contrast, the highest ethylene selectivity (56.6%) was obtained from 10%Ni_2P/TiO_2 catalyst. In addition, a much lower hydrogenolysis product (methane) was observed (~0.8% selectivity). Though, the conversion is lower than supported metallic Ni catalyst. This could suggest that Ni_2P species could selectively activate the C-H bond leading to dehydrogenation product (ethylene). Such high selective C-H activation could due to the lower nature of metallic Ni in Ni_2P.

Table 2. Conversion and product yields obtained from catalytic steam cracking of ethane [a]

Entry	Condition	Conversion (%)	Selectivity (%)			
			Methane	Ethylene	C6+	Coke
1	Thermal	1.9	0.0	40.2	59.8	0.0
2	TiO_2(P25)	2.5	0.8	30.0	69.2	0.0
3	10%Ni/TiO_2	96.1	97.5	0.0	2.1	0.4
4	10%Ni_2P/TiO_2	7.5	0.8	56.6	20.7	22.0

[a] Condition; T = 650°C, P = 1 atm, W/F = 3.55 g.h/mol

4. Conclusion

The catalytic steam cracking of ethane to ethylene on nickel phosphide catalysts supported on Titania (P25) was studied using a fixed-bed reactor, as compared to metallic Ni and TiO_2. The presence of Ni_2P species in 10%Ni_2P/TiO_2 catalysts was confirmed by XRD, H_2-TPR and *in situ* XANES. The conversion of ethane steam cracking is in the order of Thermal < TiO_2 (P25) < 10%Ni_2P/TiO_2 < 10%Ni/TiO_2 (1.9, 2.6, 6.4, 94.2%, respectively). Ni_2P species can selectively promote the C-H activation; while, metallic Ni facilitates C-C breaking.

Acknowledgements

The authors would like to acknowledge the Catalytic Chemistry Research Unit and the Department of Chemistry, Faculty of Science, KMITL. This work is partially financially supported by SCG Chemicals and TRXAS, Synchrotron Light Research Institute (SLRI), Thailand : BL2.2.

References

1. López, E.; Heracleous, E; Lemonidou, A. A.; Borio, D. O. *Chem. Eng. J.* **2008**, *145*, 308-315.
2. Mokrani, T.; Scurrell, M. *Catal. Rev.* **2012**, *51*, 1-145.
3. Vengosh, A.; Jackson, R. B.; Warner, N.; Darrah, T. H.; Kondash, A. *Environ. Sci. Technol.* **2014**, *48*, 8334-8348.
4. Froment, G. F.; Van de Steene, B. O.; Van Damme, P. S. *Ind. Eng. Chem., Process Des. Dev.* **1976**, *15*, 495-584.
5. Baria, O. A.; Holmen, A.; Blekkan, E. A. *J. Catal.* **1996**, *158*, 1-12.
6. Chin, S. Y.; Chin, Y. H.; Amiridis, M. D. *Appl. Catal.* **2006**, *300*, 8-16.
7. Sarris, S. A.; Olahova, N.; Verbeken, K.; Reyniers, M. F.; Marin, G. B.; Van Gee, K. M. *Ind. Eng. Chem. Res.* **2017**, *56*, 1424-1438.
8. Pinilla, J. L.; Arcelus-Arrillaga, P.; Puron, H.; Millan, M. *Appl. Catal.*. **2013**, *459*, 17-25.
9. Dutta, R. P.; McCaffrey, W. C.; Gray, M. R. *Energy & Fuels*. **2000**, *14*, 671-676.
10. Yang, L.; Li, X.; Wang, A.; Prins, R.; Wang, Y.; Chen, Y.; Duan, X. *J. Catal.* **2014**, *317*, 144-152.
11. Liu, P.; Rodriguez, J. A.; Takahashi, Y.; Nakamura, K. *J. Catal.* **2009**, *262*, 294-303.
12. Alvarez-Galvan, M. C.; Campos-Martin, J. M.; Fierro, J. L. G. *Catalysts*. **2019**, *293*, 1-27.
13. Chen, H.; Tan, J.; Zhu, Y.; Li, Y. Chen, H., Tan, J., Zhu, Y., & Li, Y. *Catalysis Communications*. **2016**, *73*, 46–49.
14. Seo, H. R.; Cho, K. S.; Lee, Y. K. *Mater. Sci. Eng.* **2011**, *176*, 132-140.
15. Oyama, S. T.; Wang, X.; Lee, Y. K.; Bando, K.; Requejo, F. G. *J. Catal.* **2002**, *210*, 207-217.
16. Zhang, R.; Russo, P. A.; Feist, M.; Amsalem, P.; Koch, N.; Pinna, N. *ACS Appl. Mater. Interfaces*. **2017**, *16*, 14013-14022.
17. Shamanaev, I. V.; Deliy, I. V.; Aleksandrov, P. V.; Gerasimov, E. Y.; Pakharukova, V. P.; Kodenev, E. G.; Ayupov, A. B.; Andreev, A. S.; Lapina, O. B.; Bukhtiyarova, G. A. *RSC Adv.* **2016**, *6*, 30372-30383.